Interplay of Lorentz-Berry forces in position-momentum spaces for valley-dependent impurity scattering in α-T_3 lattices

Danhong Huang,[1] Andrii Iurov,[2] Hong-Ya Xu,[3] Ying-Cheng Lai,[3,4] and Godfrey Gumbs[5]

[1]*Air Force Research Laboratory, Space Vehicles Directorate, Kirtland Air Force Base, New Mexico 87117, USA*
[2]*Center for High Technology Materials, University of New Mexico, 1313 Goddard St SE, Albuquerque, New Mexico 87106, USA*
[3]*School of Electrical, Computer and Energy Engineering, Arizona State University, Tempe, Arizona 85287, USA*
[4]*Department of Physics, Arizona State University, Tempe, Arizona 85287, USA*
[5]*Department of Physics and Astronomy, Hunter College of the City University of New York, 695 Park Avenue, New York, New York 10065, USA*

The Berry-phase mediated valley-selected skew scattering in α-T_3 lattices is demonstrated. The interplay of Lorentz and Berry forces in position and momentum spaces is revealed and analyzed. Many-body screening of the electron-impurity interaction is taken into account to avoid overestimation of back and skew scattering of electrons in the system. Triplet peak from skew interactions at two valleys is found in near-vertical and near-horizontal forward- and backward-scattering directions for small Berry phases and low magnetic fields. Magnetic-field dependence in both nonequilibrium and thermal-equilibrium currents is also presented for valley-dependent longitudinal and transverse transports mediated by a Berry phase. Mathematically, two Boltzmann moment equations are employed for computing scattering-angle distributions of nonequilibrium skew currents by using microscopic inverse energy- and momentum-relaxation times. Meanwhile, a valley-dependent unbalanced thermal-equilibrium anomalous Hall current induced by the Berry force in momentum space, due to different mobilities for two valleys, is also computed for comparisons.

I. INTRODUCTION

In electronics or spintronics [1], information is encoded through either charge or spin. Valley quantum numbers, on the other hand, become another way to distinguish and designate quantum states of a crystal lattice, which leads to the so-called valleytronics [2,3] and has already attracted a lot of interest [4–10] from both fundamental research and application perspectives. Physically speaking, valleytronics bases itself on controlling the valley degree-of-freedom of certain semiconductors with multiple valleys inside their first Brillouin zone, such as Γ, K, L, and M band-extreme points. As a comparison, electron spins have already been used for storing, manipulating, and reading out bits of information [11]. Therefore, we expect valleytronics will also demonstrate similar functionalities through multiple band extrema, where the information of 0s and 1s could be stored as discrete crystal momenta.

The valley electronic properties of solids have acquired a long history back to the early days of silicon electronics. As an example, the sixfold valley degeneracy was initially observed in electron inversion layers on (111) surfaces of silicon [12]. Later, intervalley gap anomaly was further found in two-dimensional electron gases in silicon under a strong tilted magnetic field [13]. Moreover, similar valley splitting for two-dimensional electrons has also been studied in AlAs semiconductor materials [14].

By taking graphene [15] as an example, its two nonequivalent valleys can be described as an ideal two-state system (similar to the isospin degree of freedom), and its two nonequivalent Dirac points, K and K' in the first Brillouin zone, are associated with distinct momenta or valley quantum numbers. These two valleys are well separated by a very large crystal momentum, and therefore become robust against usual external perturbations at room temperature. Quantum manipulation of valleys in semiconductors has just been demonstrated recently [16], and electrons belonging to different valleys are employed for quantum-information processing. Beyond graphene, valley characteristics are also present in other two-dimensional materials such as silicene, germanene, MoS_2, WSe_2, etc.

By looking from a technical perspective, a key issue in valleytronics turns out to be the separation of electrons with different valley quantum numbers in either position or momentum space, i.e., the so-called valley filters [2]. One way to obtain valley filtering is based on the valley Hall effect (VHE) [16], where electrons from different valleys can be separated spatially. There are other physical phenomena, e.g., the anomalous Hall effect (AHE) [17] and the spin Hall effect (SHE) [18], which are closely related to VHE. In fact, SHE has already been proven as a connection between the electrical and spin currents and can be used for spin-current generation and detection electrically in spintronics. In a similar way, we expect VHE can also generate transverse valley currents in position space like SHE.

The α-T_3 physics model is recognized as the most recent and promising candidate for novel two-dimensional materials. Its low-energy dispersions. including a flat band, can be found from a three-component generalization of the standard Dirac-Weyl Hamiltonian [19–21] and acquires a close similarity when compared with graphene [22–24]. The experimental
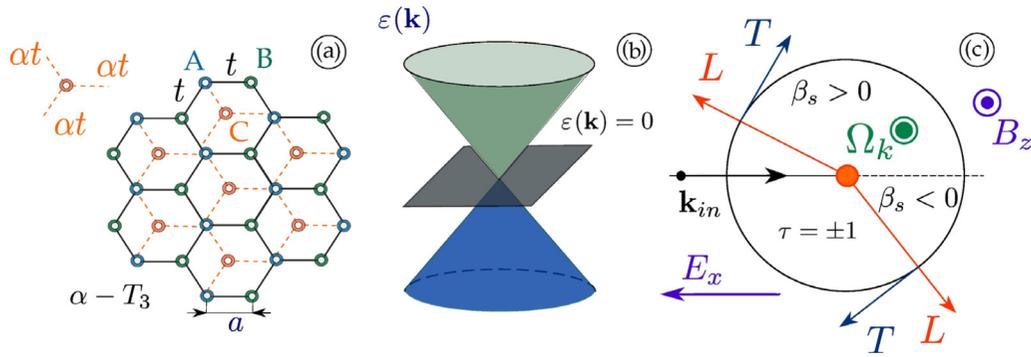
FIG. 1. (a) α-T_3 lattice with three atoms (A, B, C) per unit cell within the (x, y) plane, where the $\alpha = \tan\phi$ parameter characterizes the ratio of the bonding strengths between A-C and A-B atoms. (b) Illustration for a band structure featuring three bands of α-T_3 lattice, where the middle one is flat. (c) Schematic diagram for a scattering angle β_s of an incident electron with wave vector $\mathbf{k}_{in}$ by different impurities at two valleys characterized by $\tau = \pm 1$ under an applied electric field $\boldsymbol{E}_x$ along the x direction, where an external nonquantizing magnetic field $\boldsymbol{B}_z$, and the internal Berry curvature $\boldsymbol{\Omega}_k$ as well, are along the z direction and the longitudinal (transverse) scattering is labeled by L (T), respectively. Here the Berry phases are calculated in Sec. I as $\Phi_s^\tau(\phi) = \tau\pi\cos 2\phi$ for $s = \pm 1$ and $\Phi_0^\tau(\phi) = -2\Phi_s^\tau(\phi)$. For the sake of clearness, we call the geometry phase ϕ as the "Berry phase" in this paper.

observation for a dispersionless state was confirmed [25,26] in a photonic Lieb lattice formed by a two-dimensional array of optical waveguides. This photonic Lieb lattice can support three energy bands, including a perfectly flat middle band (i.e., an infinite effective mass). Meanwhile, even the presence of topological-insulator behavior is predicted in Lieb and kagome lattices [27]. Alternatively, the realization of the Lieb lattice can be fulfilled with an optical lattice [28], which has a flat energy band as the first excited state. Furthermore, by employing accidental degeneracy, dielectric photonic crystals with zero-refractive index can be designed and fabricated that exhibit Dirac cone dispersion at the center of the Brillouin zone at a finite frequency [29,30].

The idea of highly efficient valley filtering in α-T_3 lattices with variable Berry phase, as shown schematically in Figs. 1(a) and 1(b), has been reported very recently [31] with a Berry-phase-mediated VHE, which is termed as gVHE due to the geometric nature of the underlying mechanism. In this case, the Berry phase in momentum space can be fractionally quantized, and charge-neutral valley currents occur through skew scattering by the usual thermally ionized donor or acceptor impurities. Furthermore, a physical understanding is sought for resonant valley filtering [32] assisted by skew scattering to ensure gVHE could be robust against both thermal fluctuations and structural disorders as a result of large intervalley momentum separation.

Since novel two-dimensional (2D) materials span the full range of electronic properties, including insulators, semiconductors, semimetals, and metals, we hope to stack them layer by layer through van der Waals forces so as to build various compact planar electronic devices with high and multifunctional performance, lightweight, low-power consumption, flexibility, and even transparency. The semiconducting 2D monolayer gives rise to excellent gate control in field-effect transistors (FETs) with much shorter gate lengths (or smaller and faster transistors). Furthermore, by aligning the material's low-effective-mass lattice direction with the FET's transport, the carrier mobility will be enhanced greatly along with a high carrier density. Recent theoretical and experi-

mental endeavors on the charge transfer across a 2D material interface lead to the successful fabrication of low-resistance contacts, where the covalently bonded in-plane interfaces between different 2D materials demonstrate hope for reducing contact resistances, power consumption, and heat generation.

In this paper, our previous single-particle quantum-mechanical theory [31] for α-T_3 lattices with variable Berry phases will be generalized into a many-body quantum-statistical theory based on a generalized Boltzmann transport formalism, which microscopically calculates the inverse energy-relaxation time using the screened second-order Born approximation, the inverse momentum-relaxation-time tensor for electron elastic scattering by ionized donor and acceptor impurities, and the generalized mobility tensor based on the force-balance equation. Moreover, the zeroth- and first-order moment equations derived from the general Boltzmann transport equation will be employed for computing both the forward- and backward-scattering (near-horizontal) and skew-scattering (near-vertical) currents. Furthermore, the interplay between Lorentz and Berry forces acting on electrons in position and momentum space for both nonequilibrium and thermal-equilibrium currents is analyzed and explained.

The rest of this paper is organized as follows. In Sec. II we derive the zeroth- and first-order Boltzmann moment equations for calculating both nonequilibrium back- and skew-scattering currents in α-T_3 lattices as well as thermal-equilibrium anomalous Hall current. Meanwhile, both energy- and momentum-relaxation times are computed microscopically. In Sec. III we present numerical results for valley-dependent distributions of longitudinal and transverse currents with respect to different scattering directions, and valley-dependent 2D contour plots for partial back- and skew-scattering currents as a function of both magnetic field and Berry phase at several scattering angles. We also display in this section the total back- and skew-scattering currents in individual valleys as a function of magnetic field for different Berry phases. Finally, a summary and some remarks are presented in Sec. IV.

II. MODEL AND THEORY

The single-particle Hamiltonian [19,31] for an α-T_3 lattice takes the form of $\overleftrightarrow{\mathcal{H}}_0(\mathbf{k}_\parallel) = \hbar v_F \overleftrightarrow{\alpha} \cdot \mathbf{k}_\parallel$, where v_F and $\mathbf{k}_\parallel = \{k_x, k_y\}$ are the Fermi velocity and wave vector of electrons, $\overleftrightarrow{\alpha} = \{\overleftrightarrow{\tau}_3 \otimes \overleftrightarrow{S}_x^\alpha, \; \overleftrightarrow{\tau}_0 \otimes \overleftrightarrow{S}_y^\alpha\}$, $\overleftrightarrow{\tau}_{1,2,3}$ are three Pauli matrices, $\overleftrightarrow{\tau}_0 = \overleftrightarrow{I}_{2\times2}$ is the identity matrix corresponding to valley degree of freedom

$$\overleftrightarrow{S}_x^\alpha = \begin{bmatrix} 0 & \cos\phi & 0 \\ \cos\phi & 0 & \sin\phi \\ 0 & \sin\phi & 0 \end{bmatrix},$$

$$\overleftrightarrow{S}_y^\alpha = \begin{bmatrix} 0 & -i\cos\phi & 0 \\ i\cos\phi & 0 & -i\sin\phi \\ 0 & i\sin\phi & 0 \end{bmatrix}, \quad (1)$$

and $\alpha = \tan\phi$ $(0 \leqslant \alpha \leqslant 1)$ to parametrize the α-T_3 lattice. For this Hamiltonian, three eigenvalues are $\varepsilon_s(k_\parallel) = s\hbar v_F k_\parallel$ with $s = 0, \pm 1$ as the band index, and the associated eigenstates are

$$|s, \tau, \mathbf{k}_\parallel\rangle_\phi = \frac{1}{\sqrt{2}} \begin{bmatrix} \tau \cos\phi \, e^{-i\tau\theta_{\mathbf{k}_\parallel}} \\ s \\ \tau \sin\phi \, e^{i\tau\theta_{\mathbf{k}_\parallel}} \end{bmatrix} |\tau\rangle \quad (2)$$

for valley-degenerate eigenvalues $\varepsilon_\pm(k_\parallel) = \pm\hbar v_F k_\parallel$ [recorded as (c) for $s = +1$ and (v) for $s = -1$], and

$$|0, \tau, \mathbf{k}_\parallel\rangle_\phi = \begin{bmatrix} \tau \sin\phi \, e^{-i\tau\theta_{\mathbf{k}_\parallel}} \\ 0 \\ -\tau \cos\phi \, e^{i\tau\theta_{\mathbf{k}_\parallel}} \end{bmatrix} |\tau\rangle \quad (3)$$

for $\varepsilon_0(k_\parallel) = 0$, where $\theta_{\mathbf{k}_\parallel} = \tan^{-1}(k_y/k_x)$, and $|\tau = \pm 1\rangle$ represent two different valley states. The Berry connection [33] (field) of each band is defined as the quantum-mechanical average of the position operator $\hat{\mathbf{r}} = i\hat{\nabla}_{\mathbf{k}_\parallel}$, i.e., $A_s^{\tau,\phi}(\mathbf{k}_\parallel) = {}_\phi\langle s, \tau, \mathbf{k}_\parallel | i\hat{\nabla}_{\mathbf{k}_\parallel} | s, \tau, \mathbf{k}_\parallel\rangle_\phi$ and we get from Eqs. (2) and (3) that

$$A_0^{\tau,\phi}(\mathbf{k}_\parallel) = -\tau \frac{1-\alpha^2}{1+\alpha^2} \nabla_{\mathbf{k}_\parallel} \theta_{\mathbf{k}_\parallel}, \quad A_s^{\tau,\phi}(\mathbf{k}_\parallel) = -\frac{1}{2} A_0^{\tau,\phi}(\mathbf{k}_\parallel). \quad (4)$$

Therefore, the Berry curvature $\mathbf{\Omega}_s^{\tau,\phi}(\mathbf{k}_\parallel) = \nabla_{\mathbf{k}_\parallel} \times A_s^{\tau,\phi}(\mathbf{k}_\parallel)$ is calculated as

$$\mathbf{\Omega}_s^{\tau,\phi}(\mathbf{k}_\parallel) = \tau \left(\frac{1-\alpha^2}{1+\alpha^2} \right) \pi \, \delta(\mathbf{k}_\parallel) \hat{\mathbf{e}}_z, \quad \mathbf{\Omega}_0^{\tau,\phi}(\mathbf{k}_\parallel) = -2 \, \mathbf{\Omega}_s^{\tau,\phi}(\mathbf{k}_\parallel), \quad (5)$$

where $\hat{\mathbf{e}}_z$ is the unit coordinate vector in the z direction (perpendicular to α-T_3 plane). Connecting to the Berry connection presented in Eq. (4), the Berry phases are obtained as $\Phi_s^\tau(\phi) = \oint d\mathbf{k}_\parallel \cdot A_s^{\tau,\phi}(\mathbf{k}_\parallel) = \tau\pi \cos 2\phi$ for $s = \pm 1$ and $\Phi_0^\tau(\phi) = -2\Phi_s^\tau(\phi)$. For clearness, we simply call the geometry phase ϕ as the "Berry phase" in this paper.

For linear transport of electrons in an n-doped two-dimensional (2D) α-T_3 lattice, we start with the semiclassical Boltzmann transport equation for doped electrons in a conduction band $\varepsilon(k_\parallel) = \hbar v_F k_\parallel$ of this 2D material. In this case, the electron distribution function $f_\tau(\mathbf{r}_\parallel, \mathbf{k}_\parallel; t)$ in

position-momentum spaces satisfies [34]

$$\frac{\partial f_\tau(\mathbf{r}_\parallel, \mathbf{k}_\parallel; t)}{\partial t} + \left\langle \frac{d\mathbf{r}_\parallel(t)}{dt} \right\rangle_{\text{av}} \cdot \nabla_{\mathbf{r}_\parallel} f_\tau(\mathbf{r}_\parallel, \mathbf{k}_\parallel; t)$$
$$+ \left\langle \frac{d\mathbf{k}_\parallel(t)}{dt} \right\rangle_{\text{av}} \cdot \nabla_{\mathbf{k}_\parallel} f_\tau(\mathbf{r}_\parallel, \mathbf{k}_\parallel; t) = \left. \frac{\partial f_\tau(\mathbf{r}_\parallel, \mathbf{k}_\parallel; t)}{\partial t} \right|_{\text{coll}}, \quad (6)$$

where $\tau = \pm 1$ characterize two inequivalent valleys $\mathbf{K}$ and $\mathbf{K}'$, $\mathbf{r}_\parallel = \{x, y\}$ and $\mathbf{k}_\parallel = \{k_x, k_y\}$ are 2D position and wave vector, respectively. The term on the right-hand side of Eq. (6) corresponds to all collision contributions of electrons with ionized impurities, phonons, other electrons, etc. Moreover, for electrons, we get their group velocities through $\mathbf{v}(\mathbf{k}_\parallel) = (1/\hbar)\nabla_{\mathbf{k}_\parallel} \varepsilon(k_\parallel) = (\mathbf{k}_\parallel/k_\parallel) v_F$. Meanwhile, we find semiclassically that [35] $\langle d\mathbf{r}_\parallel(t)/dt \rangle_{\text{av}} = \mathbf{v}(\mathbf{k}_\parallel) - d\bar{\mathbf{K}}_0(t)/dt \times \mathbf{\Omega}_\perp(\mathbf{k}_\parallel) \equiv \mathbf{v}^*(\mathbf{k}_\parallel, t)$, where $\mathbf{v}^*(\mathbf{k}_\parallel, t)$ contains the so-called anomalous group velocity [33], $\bar{\mathbf{K}}_0(t)$ is the center-of-mass wave vector, $\mathbf{\Omega}_\perp(\mathbf{k}_\parallel) = \nabla_{\mathbf{k}_\parallel} \times \bar{\mathbf{R}}_0(\mathbf{k}_\parallel)$ is called the Berry curvature, and $\bar{\mathbf{R}}_0(\mathbf{k}_\parallel) = \langle \mathbf{k}_\parallel | \hat{\mathbf{r}} | \mathbf{k}_\parallel\rangle = \langle \mathbf{k}_\parallel | i\hat{\nabla}_{\mathbf{k}_\parallel} | \mathbf{k}_\parallel\rangle$ is called the Berry connection and related to the quantum-mechanical average of the center-of-mass position operator with respect to Bloch states $|\mathbf{k}_\parallel\rangle$ of a conduction band under the adiabatic condition [33]. Furthermore, we introduce a semiclassical Newton-type force equation [34] for the wave vector of electrons, yielding $\langle d\mathbf{k}_\parallel(t)/dt \rangle_{\text{av}} = (1/\hbar)\langle \mathbf{F}_{\text{em}}(\mathbf{k}_\parallel, t) \rangle_{\text{av}} = -(e/\hbar)\langle [\mathbf{E}_\parallel(t) + \mathbf{v}(\mathbf{k}_\parallel) \times \mathbf{B}_\perp(t)] \rangle_{\text{av}}$, where $\mathbf{E}_\parallel(t)$ and $\mathbf{B}_\perp(t)$ are external time-dependent electric and magnetic fields, respectively, and $\mathbf{F}_{\text{em}}(\mathbf{k}_\parallel, t)$ is the electromagnetic force acting on an electron in the $\mathbf{k}_\parallel$ state. Here $\mathbf{B}_\perp(t)$ is assumed as a nonquantizing magnetic field with Landau-level separation $\sim\hbar\omega_c$ smaller than the level lifetime broadening $\hbar/\bar{\tau}$, where ω_c denotes the associated cyclotron frequency. On the other hand, both the longitudinal and Hall conductivities for magnetoquantum transport of electrons in α-T_3 lattice have been calculated by using the Kubo formula [36].

Based on Eq. (6), the zeroth-order Boltzmann moment equation [37–40] can be obtained simply by summing over all $\mathbf{k}_\parallel$ states on both sides of this equation. After ignoring the intervalley scattering at low temperatures with a very large transition momentum, this gives rise to the electron number conservation equation, i.e., $\partial\rho/\partial t + \nabla_{\mathbf{r}_\parallel} \cdot \mathbf{J} = 0$, where the number of electrons $\rho(\mathbf{r}_\parallel, t)$ per area, as well as the particle-number current $\mathbf{J}(\mathbf{r}_\parallel, t)$ per length, are defined by $\rho(\mathbf{r}_\parallel, t) = \frac{2}{\mathcal{S}}\sum_{\tau,\mathbf{k}_\parallel} f_\tau(\mathbf{r}_\parallel, \mathbf{k}_\parallel; t)$ and $\mathbf{J}(\mathbf{r}_\parallel, t) = \frac{2}{\mathcal{S}}\sum_{\tau,\mathbf{k}_\parallel} \mathbf{v}^*(\mathbf{k}_\parallel, t) f_\tau(\mathbf{r}_\parallel, \mathbf{k}_\parallel; t)$ with $\mathcal{S}$ as the sheet area.

For the first-order Boltzmann moment equation, on the other hand, we have to employ the so-called Fermi kinetics [37–40]. For this purpose, we first introduce the energy-relaxation-time approximation for collisions, given explicitly by

$$\left. \frac{\partial f_\tau(\mathbf{r}_\parallel, \mathbf{k}_\parallel; t)}{\partial t} \right|_{\text{coll}} = -\frac{f_\tau(\mathbf{r}_\parallel, \mathbf{k}_\parallel; t) - f_T^{(0)}[\varepsilon(k_\parallel)]}{\tau_\phi(\mathbf{k}_\parallel, \tau)}, \quad (7)$$

which conserves the particle number, where $f_T^{(0)}(x) = \{1 + \exp[(x - u_0)/k_B T]\}^{-1}$ is the Fermi function for electrons in thermal-equilibrium states, T is the sample

temperature, $u_0(T)$ is the chemical potential for doped electrons, and $\tau_\phi(\mathbf{k}_\parallel, \tau)$ is the microscopic and valley-dependent energy-relaxation time for electrons in the $\mathbf{k}_\parallel$ state. The detailed quantum-statistical calculation of $\tau_\phi(\mathbf{k}_\parallel, \tau)$ can be found in Appendix C. The chemical potential $u_0(T)$ of a canonical system should be determined self-consistently by the constraint: $4 \sum_{\mathbf{k}_\parallel} f_T^{(0)}[\varepsilon(k_\parallel)] = \int d^2\mathbf{r}_\parallel \, \rho(\mathbf{r}_\parallel, t) \equiv \frac{2}{S} \sum_{\tau,\mathbf{k}_\parallel} \int d^2\mathbf{r}_\parallel f_\tau(\mathbf{r}_\parallel, \mathbf{k}_\parallel; t) = N_0 = \rho_0 S$, where N_0 and ρ_0 represent the fixed total number of spin-degenerate electrons and the electron areal density. Finally, applying this energy relaxation-time approximation to Eq. (6), we arrive at

$$f_\tau(\mathbf{r}_\parallel, \mathbf{k}_\parallel; t) + \bar{\tau}_\phi(T, \tau) \frac{\partial f_\tau(\mathbf{r}_\parallel, \mathbf{k}_\parallel; t)}{\partial t}$$

$$\approx f_T^{(0)}[\varepsilon(k_\parallel)] - \frac{\bar{\tau}_\phi(T, \tau)}{\hbar} \langle \mathbf{F}_{\text{em}}(\mathbf{k}_\parallel, t) \rangle \cdot \nabla_{\mathbf{k}_\parallel} f_T^{(0)}[\varepsilon(k_\parallel)]$$

$$- \bar{\tau}_\phi(T, \tau) \, \mathbf{v}^*(\mathbf{k}_\parallel) \cdot \nabla_{\mathbf{r}_\parallel} f_T^{(0)}[\varepsilon(k_\parallel)]$$

$$= f_T^{(0)}[\varepsilon(k_\parallel)] - \frac{\bar{\tau}_\phi(T, \tau)}{\hbar} \langle \mathbf{F}(\mathbf{k}_\parallel, t) \rangle \cdot \nabla_{\mathbf{k}_\parallel} f_T^{(0)}[\varepsilon(k_\parallel)], \quad (8)$$

where we have assumed T and u_0 are spatially uniform within the sample, and the thermally averaged and valley-dependent energy-relaxation time $\bar{\tau}_\phi(T, \tau)$ is defined by $\frac{1}{\bar{\tau}_\phi(T,\tau)} = \frac{2}{N_0} \sum_{\mathbf{k}_\parallel} \frac{f_T^{(0)}[\varepsilon(k_\parallel)]}{\tau_\phi(\mathbf{k}_\parallel, \tau)}$. By introducing another microscopic inverse momentum-relaxation-time tensor $\overset{\leftrightarrow}{\mathcal{T}}_p^{-1}(\tau, \phi)$, we can further rewrite the force-balance equation [41] for

the macroscopic center-of-mass wave vector $\mathbf{K}_0^{\tau,\phi}(t)$ in steady states as

$$\frac{d\mathbf{K}_0^{\tau,\phi}(t)}{dt} = -\overset{\leftrightarrow}{\mathcal{T}}_p^{-1}(\tau, \phi) \cdot \mathbf{K}_0^{\tau,\phi}(t) + \frac{1}{\hbar} \mathbf{F}_{\tau,\phi}(t)$$

$$= -\overset{\leftrightarrow}{\mathcal{T}}_p^{-1}(\tau, \phi) \cdot \mathbf{K}_0^{\tau,\phi}(t)$$

$$- \frac{e}{\hbar} \left\{ \mathbf{E}_\parallel(t) + \left(\frac{v_F}{k_F}\right) \mathbf{K}_0^{\tau,\phi}(t) \times \mathbf{B}_\perp(t) \right\} = 0, \quad (9)$$

where $\mathbf{F}_{\tau,\phi}(t) \equiv \langle \mathbf{F}_{\text{em}}(\mathbf{k}_\parallel, t) \rangle_{\text{av}} = -e\{\mathbf{E}_\parallel(t) + (v_F/k_F) \mathbf{K}_0^{\tau,\phi}(t) \times \mathbf{B}_\perp(t)\}$ is the macroscopic electromagnetic force, and $k_F = \sqrt{\pi \rho_0}$ is the Fermi wave number. The detailed quantum-statistical calculation of the inverse momentum-relaxation-time tensor $\overset{\leftrightarrow}{\mathcal{T}}_p^{-1}(\tau, \phi)$ is provided in Appendix D. The solution of Eq. (9) can be formally expressed as $\mathbf{K}_0^{\tau,\phi}(t) = (k_F/v_F) \overset{\leftrightarrow}{\mu}_{\tau,\phi}(\mathbf{B}_\perp(t), \overset{\leftrightarrow}{\mathcal{T}}_p^{-1}) \cdot \mathbf{E}_\parallel(t)$, where $\overset{\leftrightarrow}{\mu}_{\tau,\phi}(\mathbf{B}_\perp, \overset{\leftrightarrow}{\mathcal{T}}_p^{-1})$ is the so-called mobility tensor of electrons. The details for calculating the steady-state mobility tensor $\overset{\leftrightarrow}{\mu}_{\tau,\phi}(\mathbf{B}_\perp, \overset{\leftrightarrow}{\mathcal{T}}_p^{-1})$ are presented in Appendix E. Using this mobility tensor, we can simply write $\mathbf{F}_{\tau,\phi}(t) = (\hbar k_F/v_F) \overset{\leftrightarrow}{\mathcal{T}}_p^{-1}(\tau, \phi) \cdot \{\overset{\leftrightarrow}{\mu}_{\tau,\phi}(\mathbf{B}_\perp(t), \overset{\leftrightarrow}{\mathcal{T}}_p^{-1}) \cdot \mathbf{E}_\parallel(t)\}$.

In a similar way in deriving the zeroth-order Boltzmann moment equation, multiplying both sides of Eq. (8) by $\mathbf{v}^*(\mathbf{k}_\parallel, t)$ and summing over all electron $\mathbf{k}_\parallel$ states afterwards, we are left with the following dynamical equation:

$$\mathbf{J}_{\tau,\phi}(t) + \bar{\tau}_\phi(T, \tau) \frac{\partial \mathbf{J}_{\tau,\phi}(t)}{\partial t} = \frac{2}{S} \sum_{\mathbf{k}_\parallel} \mathbf{v}^*(\mathbf{k}_\parallel, t) f_T^{(0)}[\varepsilon(k_\parallel)] - \bar{\tau}_\phi(T, \tau) \frac{2}{S} \sum_{\mathbf{k}_\parallel} \mathbf{v}^*(\mathbf{k}_\parallel, t)[\mathbf{F}_{\tau,\phi}(t) \cdot \mathbf{v}(\mathbf{k}_\parallel)] \frac{\partial f_T^{(0)}[\varepsilon(k_\parallel)]}{\partial \varepsilon}$$

$$= \frac{2e}{\hbar S} \sum_{\mathbf{k}_\parallel} \left(\left\{\mathbf{E}_\parallel(t) + \left[\overset{\leftrightarrow}{\mu}_{\tau,\phi}(\mathbf{B}_\perp(t), \overset{\leftrightarrow}{\mathcal{T}}_p^{-1}) \cdot \mathbf{E}_\parallel(t)\right]\mathbf{B}_\perp(t)\right\} \times \mathbf{\Omega}_\perp(\mathbf{k}_\parallel)\right) f_T^{(0)}[\varepsilon(k_\parallel)]$$

$$+ \bar{\tau}_\phi(T, \tau) \left(\frac{\hbar k_F}{v_F}\right) \frac{2}{S} \sum_{\mathbf{k}_\parallel} \mathbf{v}(\mathbf{k}_\parallel) \left\{\overset{\leftrightarrow}{\mathcal{T}}_p^{-1}(\tau, \phi) \cdot \left[\overset{\leftrightarrow}{\mu}_{\tau,\phi}(\mathbf{B}_\perp(t), \overset{\leftrightarrow}{\mathcal{T}}_p^{-1}) \cdot \mathbf{E}_\parallel(t)\right]\right\}$$

$$\cdot \mathbf{v}(\mathbf{k}_\parallel) \left\{-\frac{\partial f_T^{(0)}[\varepsilon(k_\parallel)]}{\partial \varepsilon}\right\}, \quad (10)$$

where the second term on the left-hand side of the equation results from the nonadiabatic correction to the macroscopic particle-number current $\mathbf{J}_{\tau,\phi}(t)$ per length. From Eq. (10) we know $\mathbf{J}_{\tau,\phi}$ is also independent of $\mathbf{r}_\parallel$ within our approximation. As a result, from the electron number conservation equation, we find the number of electrons ρ per area must be a constant ρ_0, determined by $\rho_0 = \frac{4}{S} \sum_{\mathbf{k}_\parallel} f_T^{(0)}[\varepsilon(k_\parallel)]$, which determines the chemical potential $u_0(T)$ of the sample at any given temperature T.

If T is low, i.e., $-\frac{\partial f_T^{(0)}[\varepsilon(k_\parallel)]}{\partial \varepsilon} \approx \delta[E_F - \varepsilon(k_\parallel)]$, and external fields are assumed static $\mathbf{E}_0^\parallel$ and $\mathbf{B}_0^\perp$, we get from Eq. (10) the total charge $(-e)$ current $\mathbf{j}(\tau, \phi) = \mathbf{j}_1(\tau, \phi) + \mathbf{j}_2(\tau, \phi)$ per length for each valley, where $E_F = \hbar v_F k_F$ is the Fermi energy of electrons. Explicitly, we calculate the two current components $\mathbf{j}_1(\tau, \phi)$ and $\mathbf{j}_2(\tau, \phi)$ as

$$\mathbf{j}_1(\tau, \phi) = -\frac{e k_F^2 \bar{\tau}_\phi(k_F, \tau)}{2\pi^2 v_F^2} \int_0^{2\pi} d\theta_{\mathbf{k}_\parallel} \, \mathbf{v}(\theta_{\mathbf{k}_\parallel})\{\mathcal{T}_p^{-1}(k_F, \tau, \phi) \cdot [\overset{\leftrightarrow}{\mu}_{\tau,\phi}(\mathbf{B}_0^\perp, \overset{\leftrightarrow}{\mathcal{T}}_p^{-1}) \cdot \mathbf{E}_0^\parallel]\} \cdot \mathbf{v}(\theta_{\mathbf{k}_\parallel})$$

$$= -\frac{e k_F^2 \bar{\tau}_\phi(k_F, \tau)}{2\pi} \int_{-\pi}^{\pi} d\beta_s[\hat{\mathbf{e}}_x \mathcal{C}_x(k_F, \tau, \phi, \beta_s) + \hat{\mathbf{e}}_y \mathcal{C}_y(k_F, \tau, \phi, \beta_s)] \equiv \int_{-\pi}^{\pi} d\beta_s \, \tilde{\mathbf{j}}_1(\tau, \phi, \beta_s), \quad (11)$$

which is mediated by the Lorentz force in position space, and

$$
\begin{aligned}
\boldsymbol{j}_2(\tau,\phi) &= -\frac{e^2}{2\pi^2\hbar}\int d^2\boldsymbol{k}_\parallel\,\Theta(k_F-k_\parallel)\left\{\left[\boldsymbol{E}_0^\parallel+\left(\overset{\leftrightarrow}{\boldsymbol{\mu}}_{\tau,\phi}\left(\boldsymbol{B}_0^\perp,\overset{\leftrightarrow}{\mathcal{T}}_p^{-1}\right)\cdot\boldsymbol{E}_0^\parallel\right)\times\boldsymbol{B}_0^\perp\right]\times\boldsymbol{\Omega}_\perp(\boldsymbol{k}_\parallel)\right\} \\
&= -\frac{e^2}{2\pi^2\hbar}\int d^2\boldsymbol{k}_\parallel\,\Theta(k_F-k_\parallel)\{\hat{\boldsymbol{e}}_x[E_y-B_z(\mu_{xx}(k_F,\tau,\phi)E_x+\mu_{xy}(k_F,\tau,\phi)E_y)]\,\Omega_{\tau,\phi}(\boldsymbol{k}_\parallel) \\
&\quad -\hat{\boldsymbol{e}}_y[E_x+B_z(\mu_{yx}(k_F,\tau,\phi)E_x+\mu_{yy}(k_F,\tau,\phi)E_y)]\,\Omega_{\tau,\phi}(\boldsymbol{k}_\parallel)\} \\
&= -\frac{e^2}{2\pi^2\hbar}\left\{\frac{\tau(1-\alpha^2)\pi}{1+\alpha^2}\right\}\{\hat{\boldsymbol{e}}_x[E_y-B_z(\mu_{xx}(k_F,\tau,\phi)E_x+\mu_{xy}(k_F,\tau,\phi)E_y)] \\
&\quad -\hat{\boldsymbol{e}}_y[E_x+B_z(\mu_{yx}(k_F,\tau,\phi)E_x+\mu_{yy}(k_F,\tau,\phi)E_y)]\}\equiv j_{2x}(\tau,\phi)\hat{\boldsymbol{e}}_x+j_{2y}(\tau,\phi)\hat{\boldsymbol{e}}_y,
\end{aligned}
\tag{12}
$$

which is mediated by the Berry curvature (or Berry force) in momentum space. Here $\Theta(x)$ is a unit-step function, $\mu_{ij}(k_F,\tau,\phi)$ for $i,j=x,y$ are four elements of the mobility tensor $\overset{\leftrightarrow}{\boldsymbol{\mu}}(k_F,\tau,\phi)$ given by Eq. (18), $\boldsymbol{\Omega}_\perp(\boldsymbol{k}_\parallel)=\Omega_{\tau,\phi}(\boldsymbol{k}_\parallel)\hat{\boldsymbol{e}}_z$, $\Omega_{\tau,\phi}(\boldsymbol{k}_\parallel)=[\tau(1-\alpha^2)\pi/(1+\alpha^2)]\delta(\boldsymbol{k}_\parallel)$, $\alpha=\tan\phi$, $\theta_{\boldsymbol{k}_\parallel}=\tan^{-1}(k_y/k_x)$, $\boldsymbol{v}(\theta_{\boldsymbol{k}_\parallel})=v_F(\cos\theta_{\boldsymbol{k}_\parallel},\sin\theta_{\boldsymbol{k}_\parallel})$, and $\hat{\boldsymbol{e}}_x,\hat{\boldsymbol{e}}_y,\hat{\boldsymbol{e}}_z$ are three unit coordinate vectors. In addition, $\tilde{\boldsymbol{j}}_1(\tau,\phi,\beta_s)$ in Eq. (11) represents the extrinsic nonequilibrium scattering current along the direction of a scattering angle β_s, which is different for $\tau=1$ and -1, while $\boldsymbol{j}_2(\tau,\phi)$ in Eq. (12) is the anomalous thermal-equilibrium (extrinsic) current under doping ($E_F>0$) due to Berry curvature and independent of β_s. Furthermore, we have denoted $\mathcal{C}_{x,y}(k_F,\tau,\phi,\beta_s)$ as two spatial components of the vector $\boldsymbol{\mathcal{C}}(k_F,\tau,\phi,\beta_s)=\overset{\leftrightarrow}{\mathcal{T}}_p^{-1}(k_F,\tau,\phi,\beta_s)\cdot\{\overset{\leftrightarrow}{\boldsymbol{\mu}}(k_F,\tau,\phi)\cdot\boldsymbol{E}_0^\parallel\}$ in Eq. (11).

The elements of a conductivity tensor $\overset{\leftrightarrow}{\boldsymbol{\sigma}}(\tau,\phi,\beta_s)$ can be obtained from $\sigma_{ij}(\tau,\phi,\beta_s)=\tilde{\boldsymbol{j}}_1(\tau,\phi,\beta_s)\cdot\hat{\boldsymbol{e}}_i/(\boldsymbol{E}_0^\parallel\cdot\hat{\boldsymbol{e}}_j)$. Therefore, from Eq. (11) we know that the conductivity tensor depends not only on the mobility tensor, but also on the conduction-band energy dispersion and on how electrons are distributed within the conduction band. To elucidate scattering dynamics more clearly, we study the longitudinal $j_L(\tau,\phi)$ and transverse $j_T(\tau,\phi)$ currents which flow along and perpendicular to the direction of β_s, yielding

$$
\begin{aligned}
\begin{bmatrix}j_L(\tau,\phi)\\j_T(\tau,\phi)\end{bmatrix}&\equiv\int_{-\pi}^{\pi}d\beta_s\begin{bmatrix}j_L(\tau,\phi,\beta_s)\\j_T(\tau,\phi,\beta_s)\end{bmatrix}=-\frac{ek_F^2\bar{\tau}_\phi(k_F,\tau)}{2\pi}\int_{-\pi}^{\pi}d\beta_s\,\mathcal{C}_x(k_F,\tau,\phi,\beta_s)\begin{bmatrix}\cos\beta_s\\\sin\beta_s\end{bmatrix}\\
&\quad -\frac{ek_F^2\bar{\tau}_\phi(k_F,\tau)}{2\pi}\int_{-\pi}^{\pi}d\beta_s\,\mathcal{C}_y(k_F,\tau,\phi,\beta_s)\begin{bmatrix}\sin\beta_s\\-\cos\beta_s\end{bmatrix},
\end{aligned}
\tag{13}
$$

where the terms containing $\cos\beta_s$ select out the diagonal elements of $\overset{\leftrightarrow}{\mathcal{T}}_p^{-1}(k_F,\tau,\phi,\beta_s)$ in Eq. (16) below, while those containing $\sin\beta_s$ keep only the off-diagonal elements of $\overset{\leftrightarrow}{\mathcal{T}}_p^{-1}(k_F,\tau,\phi,\beta_s)$.

At low temperatures, from Eq. (C14) the thermally averaged energy-relaxation time $\bar{\tau}_\phi(k_F,\tau)$ introduced in Eq. (11) is given by

$$
\begin{aligned}
\frac{1}{\bar{\tau}_\phi(k_F,\tau)}&=\frac{4}{\rho_0\mathcal{S}}\sum_{\boldsymbol{k}_\parallel}\mathcal{W}_{\text{in}}^{\tau,\phi}(k_\parallel)\Theta(k_F-|\boldsymbol{k}_\parallel|)\\
&=\frac{4n_i}{\pi^2\hbar^2v_F\rho_0}\int_{-\pi}^{\pi}d\beta_s\,|\cos\theta|\int_0^{k_F}dk_\parallel\,k_\parallel^2\left|\frac{U_0^\tau(2k_\parallel|\cos\theta|)}{\epsilon_\phi(2k_\parallel|\cos\theta|)}\right|^2|\mathcal{F}_{\tau,\phi}(k_\parallel,\beta_s)|^2,
\end{aligned}
\tag{14}
$$

which depends on both $\tau=\pm1$ and $0\leqslant\phi<\pi/4$, where $|\cos\theta|=|\sin(\beta_s/2)|$, β_s is the scattering angle, $n_i=N_i/\mathcal{S}$ is the areal density of ionized impurities, and $\epsilon_\phi(q_\parallel)$ is the static dielectric function obtained from Eqs. (B6) and (B7). Meanwhile, the scattering form factor in Eq. (14) is calculated as

$$
\begin{aligned}
\mathcal{F}_{\tau,\phi}(k_\parallel,\beta_s)&=\frac{1}{2}\sum_\ell\{(-i)^{-\tau}\tau\cos\phi\,\chi_{1,\ell}^\tau(k_\parallel)+\chi_{2,\ell}^\tau(k_\parallel)+(-i)^\tau\tau\sin\phi\,\chi_{3,\ell}^\tau(k_\parallel)\}\\
&\quad\times\left\{(-i)^\tau\tau\cos\phi\,\chi_{1,\ell}^\tau(k_\parallel)\,e^{i\tau\beta_{\boldsymbol{k}_\parallel,\boldsymbol{q}_\parallel}^s}-\chi_{2,\ell}^\tau(k_\parallel)+(-i)^{-\tau}\tau\sin\phi\,\chi_{3,\ell}^\tau(k_\parallel)\,e^{-i\tau\beta_{\boldsymbol{k}_\parallel,\boldsymbol{q}_\parallel}^s}\right\}\\
&\equiv\kappa_0(k_\parallel,\phi,\tau)+\kappa_1(k_\parallel,\phi,\tau)\,e^{i\tau\beta_s}+\kappa_2(k_\parallel,\phi,\tau)\,e^{-i\tau\beta_s}+\kappa_3(k_\parallel,\phi,\tau)(1+e^{i\tau\beta_s})\\
&\quad+\kappa_4(k_\parallel,\phi,\tau)(1+e^{-i\tau\beta_s})+\kappa_5(k_\parallel,\phi,\tau)\cos(\tau\beta_s),
\end{aligned}
\tag{15}
$$

where $\chi_{1,\ell}^\tau(k_\parallel)$, $\chi_{2,\ell}^\tau(k_\parallel)$, and $\chi_{3,\ell}^\tau(k_\parallel)$ are the scattering factors defined in Eq. (C12), and six real scattering coefficients κ_j with $j=0,1,\dots,5$ can be obtained from Eq. (C13).

In addition, from Eq. (D3) the inverse momentum-relaxation-time tensor employed in Eq. (11) is microscopically calculated at low temperatures as

$$
\begin{aligned}
\overleftrightarrow{\mathcal{T}}_p^{-1}(k_F, \tau, \phi) &= \frac{2\pi n_i}{\rho_0}\left(\frac{v_F}{k_F}\right) \sum_{\mathbf{k}_\parallel, \mathbf{q}_\parallel} \left|U_{\mathrm{im}}^{\tau,\phi}(\mathbf{q}_\parallel, \mathbf{k}_\parallel)\right|^2 \delta(\varepsilon_{\mathbf{k}_\parallel} - E_F)\,\delta(\varepsilon_{\mathbf{k}_\parallel + \mathbf{q}_\parallel} - \varepsilon_{\mathbf{k}_\parallel})\,[\mathbf{q}_\parallel \otimes \mathbf{q}_\parallel^T] \\
&= \frac{2 n_i k_F^3}{\pi^2 \hbar^2 v_F \rho_0} \int_{-\pi}^{\pi} d\beta_s \, |\sin(\beta_s/2)|\sin^2(\beta_s/2) \left|\frac{U_0^\tau[2k_F|\sin(\beta_s/2)|]}{\epsilon_\phi[2k_F|\sin(\beta_s/2)|]}\right|^2 |\mathcal{F}_{\tau,\phi}(k_F, \beta_s)|^2 \\
&\quad \times \begin{bmatrix} \sin^2(\beta_s/2) & -\sin(\beta_s)/2 \\ -\sin(\beta_s)/2 & \cos^2(\beta_s/2) \end{bmatrix} \equiv \int_{-\pi}^{\pi} d\beta_s \, \overleftrightarrow{\mathcal{T}}_p^{-1}(k_F, \tau, \phi, \beta_s),
\end{aligned}
\tag{16}
$$

where $|\mathcal{F}_{\tau,\phi}(k_F, \beta_s)|^2$ has already been given by Eq. (15). It is evident from Eq. (16) that the off-diagonal elements of $\overleftrightarrow{\mathcal{T}}_p^{-1}(k_F, \tau, \phi)$ become zero after the integral has been performed with respect to β_s from $-\pi$ to π, while the diagonal elements of $\overleftrightarrow{\mathcal{T}}_p^{-1}(k_F, \tau, \phi)$ are nonzero and different simultaneously. Physically, the diagonal elements of $\overleftrightarrow{\mathcal{T}}_p^{-1}(k_F, \tau, \phi, \beta_s)$ correspond to the case in which directions of the scattering force and center-of-mass momentum are parallel to each other. The off-diagonal elements of $\overleftrightarrow{\mathcal{T}}_p^{-1}(k_F, \tau, \phi, \beta_s)$, on the other hand, are related to a situation where the direction of the scattering force is perpendicular to that of the center-of-mass momentum.

Formally, by denoting the results in Eq. (16) as

$$
\overleftrightarrow{\mathcal{T}}_p^{-1}(k_F, \tau, \phi) = \begin{bmatrix} b_{xx}(k_F, \tau, \phi) & 0 \\ 0 & b_{yy}(k_F, \tau, \phi) \end{bmatrix},
\tag{17}
$$

from Eqs. (E3) and (E5)–(E7) and $\mu_{ij}(k_F, \tau, \phi) = (v_F/k_F)\,\partial K_i^{\tau,\phi}/\partial E_j$, the mobility-tensor $\overleftrightarrow{\mu}(k_F, \tau, \phi)$ introduced in Eq. (11) can easily be found as

$$
\overleftrightarrow{\mu}(k_F, \tau, \phi) = \frac{-\dfrac{ev_F}{\hbar k_F}}{b_{xx}(k_F, \tau, \phi)\,b_{yy}(k_F, \tau, \phi) + \left(\dfrac{ev_F B_z}{\hbar k_F}\right)^2} \begin{bmatrix} b_{yy}(k_F, \tau, \phi) & -\dfrac{ev_F B_z}{\hbar k_F} \\ \dfrac{ev_F B_z}{\hbar k_F} & b_{xx}(k_F, \tau, \phi) \end{bmatrix},
\tag{18}
$$

which depends on $\tau = \pm 1$ and ϕ, where $\mathbf{B}_0^\perp = (0, 0, B_z)$ introduces a normal Hall mobility (off-diagonal elements) due to broken time-reversal symmetry. We would like to point out that the off-diagonal elements of $\overleftrightarrow{\mathcal{T}}_p^{-1}(k_F, \tau, \phi, \beta_s)$ in Eq. (16) can be nonzero in principle if an anisotropic energy dispersion $\varepsilon(\mathbf{k}_\parallel)$ contains a k_x and k_y crossing term, e.g., $\varepsilon(\mathbf{k}_\parallel) \propto k_x k_y$.

Finally, by using Eq. (18), we obtain two components of the vector $\mathbf{C}(k_F, \tau, \phi, \beta_s) = [\mathcal{C}_x(k_F, \tau, \phi, \beta_s), \mathcal{C}_y(k_F, \tau, \phi, \beta_s)] = \overleftrightarrow{\mathcal{T}}_p^{-1}(k_F, \tau, \phi, \beta_s) \cdot [\overleftrightarrow{\mu}(k_F, \tau, \phi) \cdot \mathbf{E}_0^\parallel]$ introduced in Eq. (11) as

$$
\begin{aligned}
\mathcal{C}_x(k_F, \tau, \phi, \beta_s) = &-\left(\frac{ev_F}{\hbar k_F}\right)\left\{\frac{b_{yy}(k_F, \tau, \phi)E_x - \left(\dfrac{ev_F B_z}{\hbar k_F}\right)E_y}{b_{xx}(k_F, \tau, \phi)\,b_{yy}(k_F, \tau, \phi) + \left(\dfrac{ev_F B_z}{\hbar k_F}\right)^2}\right\} d_{xx}(k_F, \tau, \phi, \beta_s) \\
&-\left(\frac{ev_F}{\hbar k_F}\right)\left\{\frac{\left(\dfrac{ev_F B_z}{\hbar k_F}\right)E_x + b_{xx}(k_F, \tau, \phi)E_y}{b_{xx}(k_F, \tau, \phi)\,b_{yy}(k_F, \tau, \phi) + \left(\dfrac{ev_F B_z}{\hbar k_F}\right)^2}\right\} d_{xy}(k_F, \tau, \phi, \beta_s),
\end{aligned}
\tag{19}
$$

$$
\begin{aligned}
\mathcal{C}_y(k_F, \tau, \phi, \beta_s) = &-\left(\frac{ev_F}{\hbar k_F}\right)\left\{\frac{\left(\dfrac{ev_F B_z}{\hbar k_F}\right)E_x + b_{xx}(k_F, \tau, \phi)E_y}{b_{xx}(k_F, \tau, \phi)\,b_{yy}(k_F, \tau, \phi) + \left(\dfrac{ev_F B_z}{\hbar k_F}\right)^2}\right\} d_{yy}(k_F, \tau, \phi, \beta_s) \\
&-\left(\frac{ev_F}{\hbar k_F}\right)\left\{\frac{b_{yy}(k_F, \tau, \phi)E_x - \left(\dfrac{ev_F B_z}{\hbar k_F}\right)E_y}{b_{xx}(k_F, \tau, \phi)\,b_{yy}(k_F, \tau, \phi) + \left(\dfrac{ev_F B_z}{\hbar k_F}\right)^2}\right\} d_{xy}(k_F, \tau, \phi, \beta_s),
\end{aligned}
\tag{20}
$$
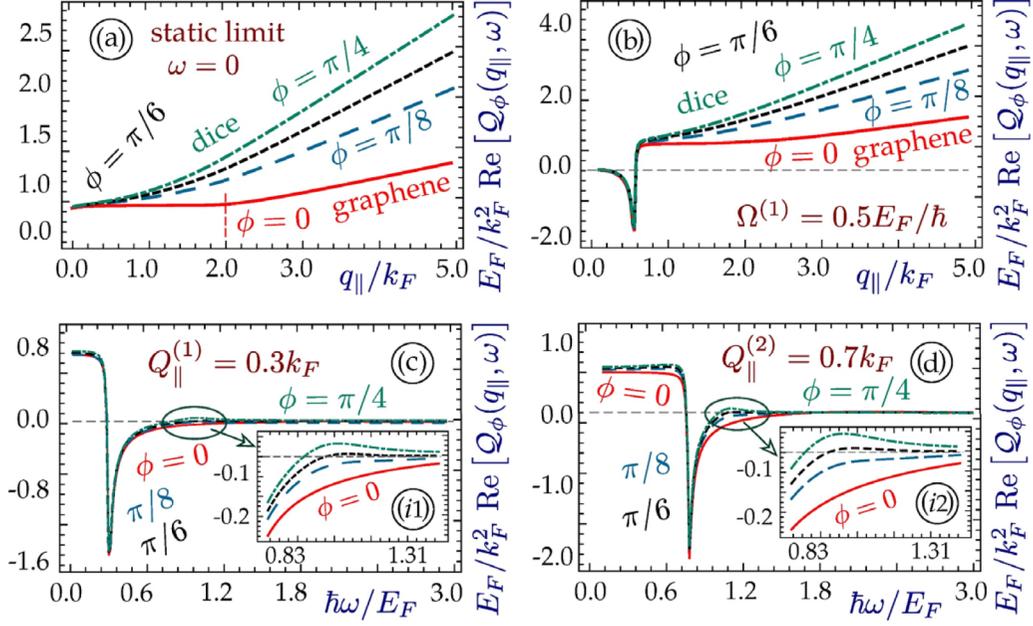
FIG. 2. Calculated real part of the polarization function $\text{Re}[\mathcal{Q}_\phi(\boldsymbol{q}_\parallel, \omega)]$ from Eq. (B2) with $\phi = \pi/4$ (dice, green), $\pi/6$ (black), $\pi/8$ (blue), and 0 (graphene, red) as a function of $q_\parallel$ at $\hbar\omega = 0$ (a) and $\hbar\omega/E_F = 0.5$ (b), as well as a function of $\hbar\omega$ at $q_\parallel/k_F = 0.3$ (c) and $q_\parallel/k_F = 0.7$ (d). Here the unit of (k_F^2/E_F) has been used for scaling $\mathcal{Q}_\phi(\boldsymbol{q}_\parallel, \omega)$ in Eq. (B2).

which depend on B_z, $\tau = \pm 1$, geometry phase ϕ, as well as on β_s, where $\boldsymbol{E}_0^\parallel = (E_x, E_y, 0)$ is assumed. In addition, $d_{xx}(k_F, \tau, \phi, \beta_s)$, $d_{yy}(k_F, \tau, \phi, \beta_s)$, and $d_{xy}(k_F, \tau, \phi, \beta_s)$ in Eq. (20) are given explicitly by

$$d_{xx}(k_F, \tau, \phi, \beta_s) = \mathcal{G}_s(k_F, \tau, \phi, \beta_s)(1 - \cos\beta_s), \quad d_{yy}(k_F, \tau, \phi, \beta_s) = \mathcal{G}_s(k_F, \tau, \phi, \beta_s)(1 + \cos\beta_s),$$

$$d_{xy}(k_F, \tau, \phi, \beta_s) = -\mathcal{G}_s(k_F, \tau, \phi, \beta_s)\sin\beta_s, \tag{21}$$

where the scattering function $\mathcal{G}_s(k_F, \tau, \phi, \beta_s)$, which depends on τ, ϕ, and β_s, is defined as

$$\mathcal{G}_s(k_F, \tau, \phi, \beta_s) = \frac{n_i k_F^3}{4\pi^2 \hbar^2 v_F \rho_0} |\sin^3(\beta_s/2)| \left| \frac{U_0^\tau[2k_F |\sin(\beta_s/2)|]}{\epsilon_\phi[2k_F |\sin(\beta_s/2)|]} \right|^2 |\mathcal{F}_{\tau,\phi}(k_F, \beta_s)|^2. \tag{22}$$

In Eqs. (19) and (20), the terms containing $d_{xy}(k_F, \tau, \phi, \beta_s)$ represent the contributions to skew scattering.

III. NUMERICAL RESULTS AND DISCUSSIONS

In our numerical calculations, $v_F = 10^8$ cm/s is the graphene Fermi velocity, $\rho_0 = 5 \times 10^{11}$ cm^{-2} the electron areal density, $k_F = \sqrt{\pi \rho_0} = 1.25 \times 10^6$ cm^{-1} the Fermi wave number of electrons, $E_F = \hbar v_F k_F = 130$ meV the electron Fermi energy, and $n_i = 2.5 \times 10^{11}$ cm^{-2} is the impurity areal density. In addition, $\epsilon_r = 13$ stands for the average dielectric constant of a host for embedding α-T_3 lattices, $V_0/E_F = 1.4$ gives rise to the step height V_0 for an impurity potential, $k_F r_0 = 7$ decides the radius r_0 of the step potential. Finally, $E_x = 0.5$ kV/cm is the applied longitudinal electric field, and $E_y = 0$ is the external transverse electric field. The other parameters, such as ϕ (geometry phase), τ (valley index), and B_z (perpendicular magnetic field), will be directly given in figure captions.

Using Eq. (B2), we have shown in Fig. 2 the real part of the polarization function $\text{Re}[\mathcal{Q}_\phi(q_\parallel, \omega)]$ as a function of $q_\parallel$ at $\hbar\omega/E_F = 0$ [Fig. 2(a)] and 0.5 [Fig. 2(b)] and as a function of $\hbar\omega$ at $q_\parallel/k_F = 0.3$ [Fig. 2(c)] and 0.7 [Fig. 2(d)]. We know from Fig. 2(a) that all results with different ϕ

approach a finite constant as $q_\parallel \to 0$ in the static limit ($\omega = 0$), including graphene with $\phi = 0$ within the whole region of $q_\parallel/k_F \leqslant 2$. However, they increase significantly with $q_\parallel$ as $q_\parallel/k_F > 2$ and become strongly ϕ dependent. These features in Fig. 2(a) change completely for $\hbar\omega/E_F = 0.5$, as shown in Fig. 2(b), where $\text{Re}[\mathcal{Q}_\phi(q_\parallel, \omega)] = 0$ (i.e., no screening) at $q_\parallel = 0$ for all values of ϕ. Figures 2(c) and 2(d) display $\text{Re}[\mathcal{Q}_\phi(q_\parallel, \omega)]$ as a function of $\hbar\omega$ at $q_\parallel/k_F = 0.3$ [Fig. 2(c)] and 0.7 [Fig. 2(d)], where a sharp and nearly ϕ-independent negative peak shifts up rapidly in frequency as $q_\parallel$ increases. Moreover, a series of intersections with the thin dashed line (i.e., $\text{Re}[\mathcal{Q}_\phi(q_\parallel, \omega)] = 0$) is seen in the two insets in Figs. 2(c) and 2(d). This highlights a sign switch of $\text{Re}[\mathcal{Q}_\phi(q_\parallel, \omega)]$ and implies the existence of a set of ϕ-dependent plasmon resonances determined from $\text{Re}[\mathcal{Q}_\phi(q_\parallel, \omega)] = -\alpha q_\parallel/k_F$ with $\alpha = 2\epsilon_0\epsilon_r \hbar v_F/e^2$ on the right-hand-side shoulder of this negative peak. As seen from the dielectric function in Eq. (B1), the nonzero flat-band part in Eq. (B2) can be obtained separately by using Eq. (B4), which represents the flat-band contribution to the screening of impurity scattering.
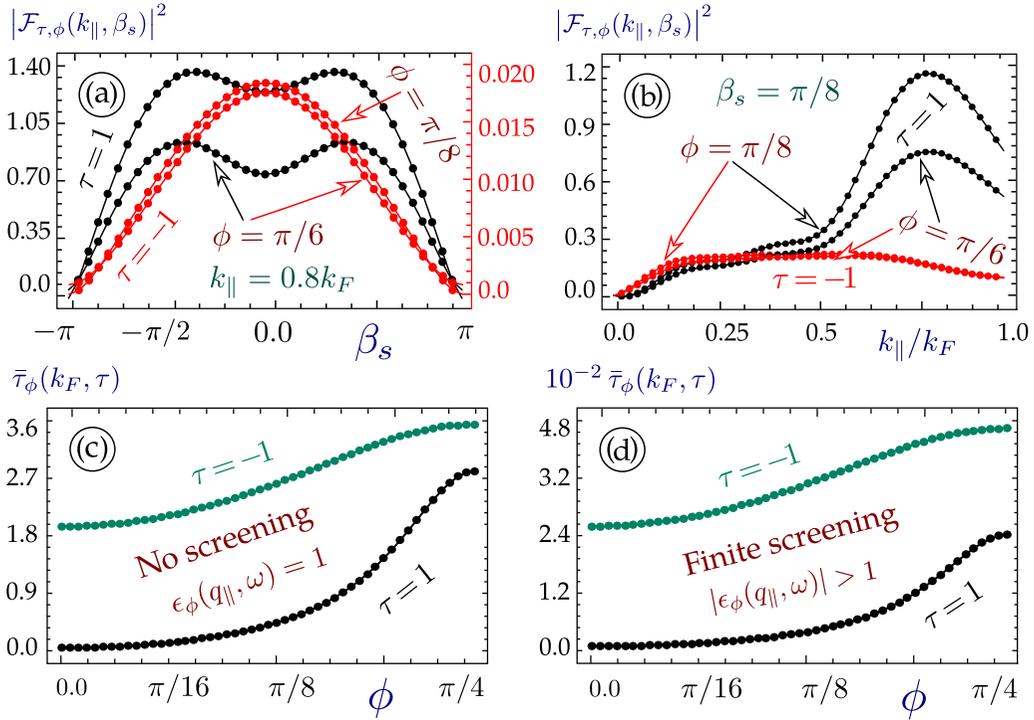
FIG. 3. Calculated square of the dimensionless form factor $|\mathcal{F}_{\tau,\phi}(k_{\parallel},\beta_s)|^2$ from Eq. (15) with $\phi = \pi/6$ and $\pi/8$ as a function of β_s at $k_{\parallel}/k_F = 0.8$ (a) and as a function of $k_{\parallel}$ at $\beta_s = \pi/8$ (b) for $\tau = 1$ (black) and $\tau = -1$ (red); as well as thermally averaged energy-relaxation time $\bar{\tau}_{\phi}(k_F, \tau)$ calculated from Eq. (14) as a function of ϕ for $\tau = 1$ (black) and $\tau = -1$ (green) under both unscreened (c) and screened (d) conditions. Here the unit of $(\pi^2\hbar/4E_F)$ has been used for scaling $\bar{\tau}_{\phi}(k_F, \tau)$.

The form factor $|\mathcal{F}_{\tau,\phi}(k_{\parallel},\beta_s)|$ defined in Eq. (15) introduces different effects from various geometry phases (ϕ) on scattering-angle (β_s) dependence for both energy-relaxation time in Eq. (14) and momentum-relaxation time in Eqs. (16) and (22) compared with special cases of graphene ($\phi = 0$) and dice lattice $\phi = \pi/4$. We present the calculated square of the form factor $|\mathcal{F}_{\tau,\phi}(k_{\parallel},\beta_s)|^2$ in Fig. 3 for $\tau = \pm 1$ by using Eq. (15) as a function of the scattering angle β_s at $k_{\parallel}/k_F = 0.8$ [Fig. 3(a)] and as a function of the wave number $k_{\parallel}/k_F$ at $\beta_s = \pi/8$ [Fig. 3(b)] with $\phi = \pi/8$ and $\pi/6$. From Fig. 3(a) we find either a single peak or double peaks with respect to β_s for $\tau = 1$ (black, left scale) or $\tau = -1$ (red, right scale), respectively. This valley-dependent behavior of $|\mathcal{F}_{\tau,\phi}(k_{\parallel},\beta_s)|^2$ is attributed to different barrierlike (traplike) impurity scattering for $\tau = 1$ ($\tau = -1$), and the latter only acquires a weak strength. Moreover, we find from Fig. 3(b) that significant difference in $|\mathcal{F}_{\tau,\phi}(k_{\parallel},\beta_s)|^2$ for $\tau = \pm 1$ exists only for large $k_{\parallel}$ values ($k_{\parallel}/k_F \geqslant 0.5$). This valley dependence of $|\mathcal{F}_{\tau,\phi}(k_{\parallel},\beta_s)|^2$ has a profound influence on the energy-relaxation time $\bar{\tau}_{\phi}(k_F, \tau)$, as demonstrated by Figs. 3(c) and 3(d), where $\bar{\tau}_{\phi}(k_F, \tau)$ calculated from Eq. (14) is displayed as a function of Berry phase ϕ for $\tau = 1$ and -1 under both unscreened [Fig. 3(c)] with $\epsilon_{\phi}(q_{\parallel}, \omega) \equiv 1$ and screened [Fig. 3(d)] conditions. By comparing Fig. 3(c) with Fig. 3(d), it is apparent that the strength of impurity scattering can be overestimated by almost two orders of magnitude if the many-body screening effect has been neglected. Meanwhile, $\bar{\tau}_{\phi}(k_F, \tau)$ increases monotonically with ϕ, and it becomes larger for $\tau = -1$, in comparison with that for $\tau = 1$, due to a weaker traplike impurity scattering of electrons. Furthermore, the difference in $\bar{\tau}_{\phi}(k_F, \tau)$

under screening for two valleys remains unchanged for all values of ϕ.

The same form factor $|\mathcal{F}_{\tau,\phi}(k_{\parallel},\beta_s)|$ also leads to a unique ϕ dependence for two diagonal elements of an inverse momentum-relaxation-time tensor in Eq. (17). The calculated two diagonal elements, $b_{xx}(k_F, \tau, \phi)$ and $b_{yy}(k_F, \tau, \phi)$, of the inverse momentum-relaxation-time tensor $\overleftrightarrow{\mathcal{T}}_p^{-1}(k_F, \tau, \phi)$ in Eq. (17) are presented in Figs. 4(a) and 4(b) as a function of ϕ for $\tau = 1$ and -1, respectively. We first notice from Fig. 4(b) that $b_{xx}(k_F, \tau, \phi)$ is lower than $b_{yy}(k_F, \tau, \phi)$, but both of them decrease monotonically with ϕ in a similar way. Also, we would like to point out that the rate difference $\delta b \equiv b_{xx}(k_F, \tau, \phi) - b_{yy}(k_F, \tau, \phi)$, as shown by the inset in Fig. 4(a), decreases with ϕ initially but switches to negative and saturates afterwards for large ϕ values. Contrary to the result in Fig. 4(b), we find $b_{xx}(k_F, \tau, \phi) > b_{yy}(k_F, \tau, \phi)$ in Fig. 4(a) before the sign switch of δb. Moreover, $b_{xx}(k_F, \tau, \phi)$ and $b_{yy}(k_F, \tau, \phi)$ in Fig. 4(a) are more than two orders of magnitude higher than those in Fig. 4(b), implying an enhanced momentum-dissipation rate for electrons at the $\tau = 1$ valley due to much larger $|\mathcal{F}_{\tau,\phi}(k_{\parallel},\beta_s)|^2$ for $\tau = 1$ and $k_{\parallel} = k_F$ in Fig. 3(b).

In Fig. 5 we exhibit two diagonal elements, $\mu_{xx}(k_F, \tau, \phi)$ [Figs. 5(a) and 5(b)] and $\mu_{yy}(k_F, \tau, \phi)$ [Figs. 5(e) and 5(f)], as well as the off-diagonal element, $\mu_{xy}(k_F, \tau, \phi)$ [Figs. 5(c) and 5(d)], of the mobility tensor $\overleftrightarrow{\mu}(k_F, \tau, \phi)$ in Eq. (18) as a function of magnetic field B_z for four different Berry phases and $\tau = \pm 1$. By comparing Figs. 5(a), 5(c), and 5(e) for $\tau = 1$ with Figs. 5(b), 5(d), and 5(f) for $\tau = -1$,
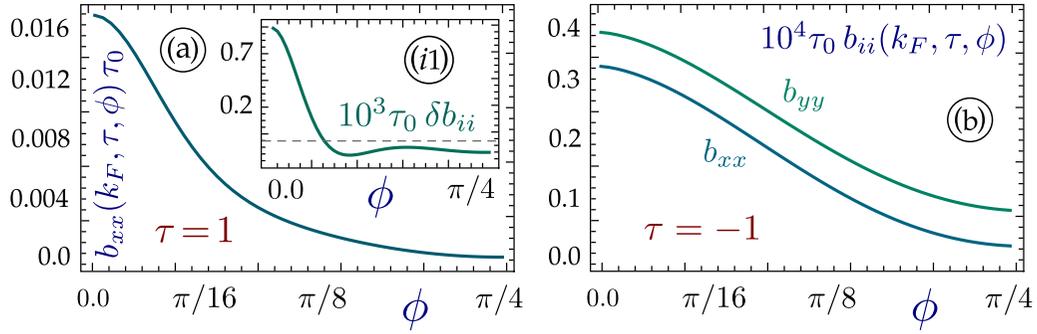
FIG. 4. Calculated diagonal elements $b_{xx}(k_F, \tau, \phi)$ for $\tau = 1$ (a) and both $b_{xx}(k_F, \tau, \phi)$ and $b_{yy}(k_F, \tau, \phi)$ for $\tau = -1$ (b) of the inverse momentum-relaxation-time tensor $\overleftrightarrow{\mathcal{T}}_p^{-1}(k_F, \tau, \phi)$ in Eq. (17) as functions of ϕ, where the difference $\delta b \equiv b_{xx}(k_F, \tau, \phi) - b_{yy}(k_F, \tau, \phi)$ for $\tau = 1$ is also presented in the inset (i1) and the dashed line corresponds to $\delta b = 0$ to highlight its sign switching. Here the unit of $1/\tau_0 = 4E_F/\pi^2\hbar$ has been used for scaling $b_{xx}(k_F, \tau, \phi)$ and $b_{yy}(k_F, \tau, \phi)$.

we discover significant difference between their dependence and magnitudes due to two orders of magnitude change in $b_{xx}(k_F, \tau, \phi)$ and $b_{yy}(k_F, \tau, \phi)$ in Fig. 4 for $\tau = 1$ and -1. The longitudinal mobilities $\mu_{xx}(k_F, \tau, \phi)$ and $\mu_{yy}(k_F, \tau, \phi)$, related to back scattering of electrons, are somewhat sup-

pressed not only by increasing the Lorentz force (or increasing B_z) in position space due to cyclotron motion, but also by decreasing the Berry force [or decreasing Berry curvature $\Omega_s^{\tau, \phi}(\boldsymbol{k}_\parallel)$] in momentum space. For high B_z, we arrive at $\mu_{xx}, \mu_{yy} \sim 1/B_z^2$, corresponding to a classical limit. In ad-
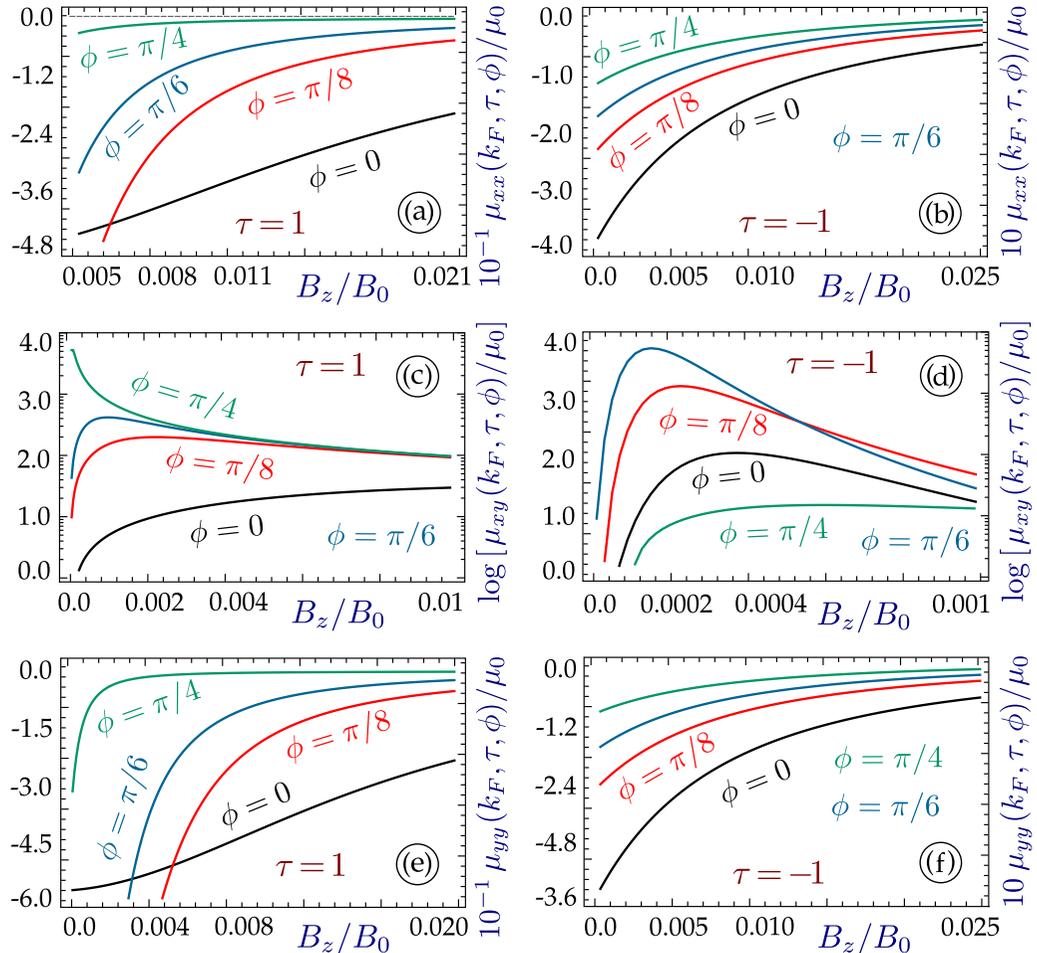
FIG. 5. Calculated diagonal elements $\mu_{xx}(k_F, \tau, \phi)$ (a) and (b) and $\mu_{yy}(k_F, \tau, \phi)$ (e) and (f), as well as off-diagonal element $\mu_{xy}(k_F, \tau, \phi)$ in logarithm scale (c) and (d), of the mobility tensor $\overleftrightarrow{\mu}(k_F, \tau, \phi)$ given by Eq. (18) as a function of B_z with $\phi = \pi/4$ (green), $\phi = \pi/6$ (blue), $\phi = \pi/8$ (red), and $\phi = 0$ (black) for $\tau = 1$ (a), (c), and (e) and $\tau = -1$ (b), (d), and (f). Here $\mu_0 = 4e/\pi^2\hbar k_F^2$ has been used for scaling all elements of $\overleftrightarrow{\mu}(k_F, \tau, \phi)$ and $B_0 = \hbar k_F^2/e$.
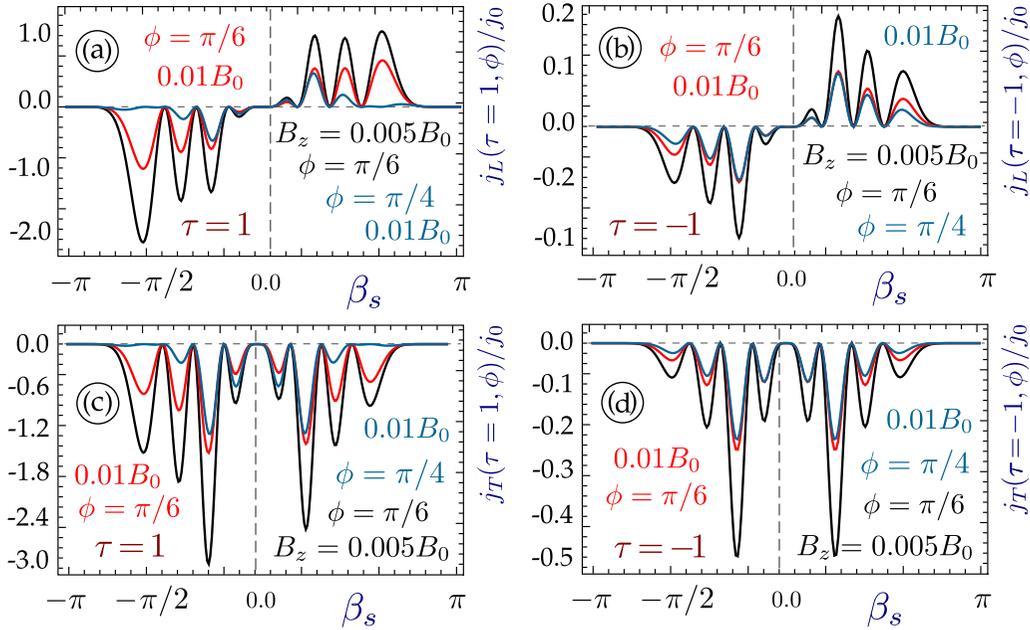
FIG. 6. Calculated integrands of longitudinal $j_L(\tau, \phi)$ (a) and (b) and transverse $j_T(\tau, \phi)$ (c) and (d) scattering currents from Eq. (13) as a function of $\beta_s \in [-\pi, \pi]$ with $\phi = \pi/4$, $B_z/B_0 = 0.01$ (blue), $\phi = \pi/6$, $B_z/B_0 = 0.01$ (red), and $\phi = \pi/6$, $B_z/B_0 = 0.005$ (black) for $\tau = 1$ (a) and (c) and $\tau = -1$ (b) and (d). Here the unit of $j_0 = n_i e v_F$ has been used for scaling both $j_L(\tau, \phi)$ and $j_T(\tau, \phi)$ and B_0 is given in Fig. 5.

dition, the transverse mobility $\mu_{xy}(k_F, \tau, \phi)$, connected to skew scattering of electrons, also decreases with reduced Berry force in momentum space at low B_z, where an initial sharp increase [logarithm scale in Figs. 5(c) and 5(d)] of $\mu_{xy}(k_F, \tau, \phi)$ is found slightly above $B_z = 0$ but it quickly changes to decreasing with B_z until a classical limit, i.e., $\mu_{xy} \sim 1/B_z$, is reached in the strong-field limit. The calculated magnetic-field dependence in both diagonal and off-diagonal elements of a mobility tensor defined in Eq. (18) can be verified experimentally by using the so-called time-of-flight technique [42].

After presenting a full calculation of physical parameters of α-T_3 lattices in Figs. 2–5, we turn to discussions on valley-dependent electrical responses, i.e., gVHE on directly measurable sheet current density. To clearly reveal valley scattering dynamics, we show in Fig. 6 the scattering-angle (β_s) distributions of longitudinal $j_L(\tau, \phi, \beta_s)$ [Figs. 6(a) and 6(b)] and transverse $j_T(\tau, \phi, \beta_s)$ [Figs. 6(c) and 6(d)] currents given by Eq. (13) with various Berry phases ϕ and B_z for $\tau = 1$ [Figs. 6(a) and 6(c)] and $\tau = -1$ [Figs. 6(b) and 6(d)]. From Figs. 6(a) and 6(b) we see a triplet peak in $j_L(\tau, \phi)$ with opposite signs for $\beta_s > 0$ and $\beta_s < 0$. Much more interestingly, we always find one backward plus one forward near-vertical (near-horizontal) scattering of electrons from two different valley impurities, characterized by $\tau = 1$ ($\tau = -1$) here. As expected, $j_L(\tau, \phi)$ for $\tau = 1$ is one order of magnitude higher than that for $\tau = -1$ because of a larger mobility for the former. The increase of B_z significantly reduces $j_L(\tau, \phi)$ at $\phi = \pi/6$ for both $\tau = \pm 1$ (black and red) due to cyclotron motion. Meanwhile, the increase of Berry phase ϕ further reduces $j_L(\tau, \phi)$ at $B_z/B_0 = 0.01$ for both $\tau = \pm 1$ (red and blue) due to decreasing Berry force. Furthermore, the negative triplet peak is always present for $j_T(\tau, \phi)$ in both $\beta_s > 0$ and $\beta_s < 0$ regions, as shown in

Figs. 6(c) and 6(d). Here $j_T(\tau, \phi)$ exhibits the same dependence as for the triplet peak in $j_L(\tau, \phi)$ on B_z and ϕ. In this case, however, one always finds a counterclockwise tangential current $j_T(\tau, \phi)$ for dominant near-horizontal forward and backward scattering of electrons with an impurity at both valleys.

In order to gain a better physics picture about the valley-dependent triplet peak of the longitudinal scattering currents in Figs. 6(a) and 6(b), we present in Fig. 7 the back-scattering current-distribution component $C_x(k_F, \tau, \phi, \beta_s)$ from Eq. (19) as a function of either B_z or β_s, as well as 2D contour plots of $C_x(k_F, \tau, \phi, \beta_s)$ as a function of both ϕ and B_z for $\tau = 1$ ($\tau = -1$) and $\beta_s = -5\pi/8$ ($\beta_s = -9\pi/40$), respectively. We find from Figs. 7(a) and 7(b) that for all cases $C_x(k_F, \tau, \phi, \beta_s)$ is initially increased but subsequently reduced by a magnetic field for both $\tau = \pm 1$. Increasing ϕ from $\pi/6$ (black) to $\pi/4$ (green) at fixed $\beta_s = \pi/6$ can switch the sign of (reduce) $C_x(k_F, \tau, \phi, \beta_s)$ for $\tau = 1$ ($\tau = -1$) at low B_z. An opposite situation occurs at $\beta_s = \pi/3$, but experiences a smaller change for $\tau = 1$. On the other hand, from Figs. 7(c) and 7(d) we see one backward plus one forward weak near-vertical (very strong near-horizontal) scattering for $\tau = 1$ ($\tau = -1$), respectively, with similar features as those found in Figs. 6(a) and 6(b) for their dependence on B_z and ϕ. The contour plot at $\beta_s = -5\pi/8$ and $\tau = 1$ in Fig. 7(e) displays an "island" in $C_x(k_F, \tau, \phi, \beta_s)$ at the left side of this panel associated with low ϕ and intermediate B_z values. For $\tau = -1$ and $\beta_s = -9\pi/40$ in Fig. 7(f), however, only a negative peak at bottom is found for very low B_z. Such distinctive features in Figs. 7(e) and 7(f) present a clear proof to the existence of gVHE in the current system.

We also plot in Fig. 8 the skew-scattering current-distribution component $C_y(k_F, \tau, \phi, \beta_s)$ from Eq. (20) as a function of B_z and β_s, as well as 2D contour plots of
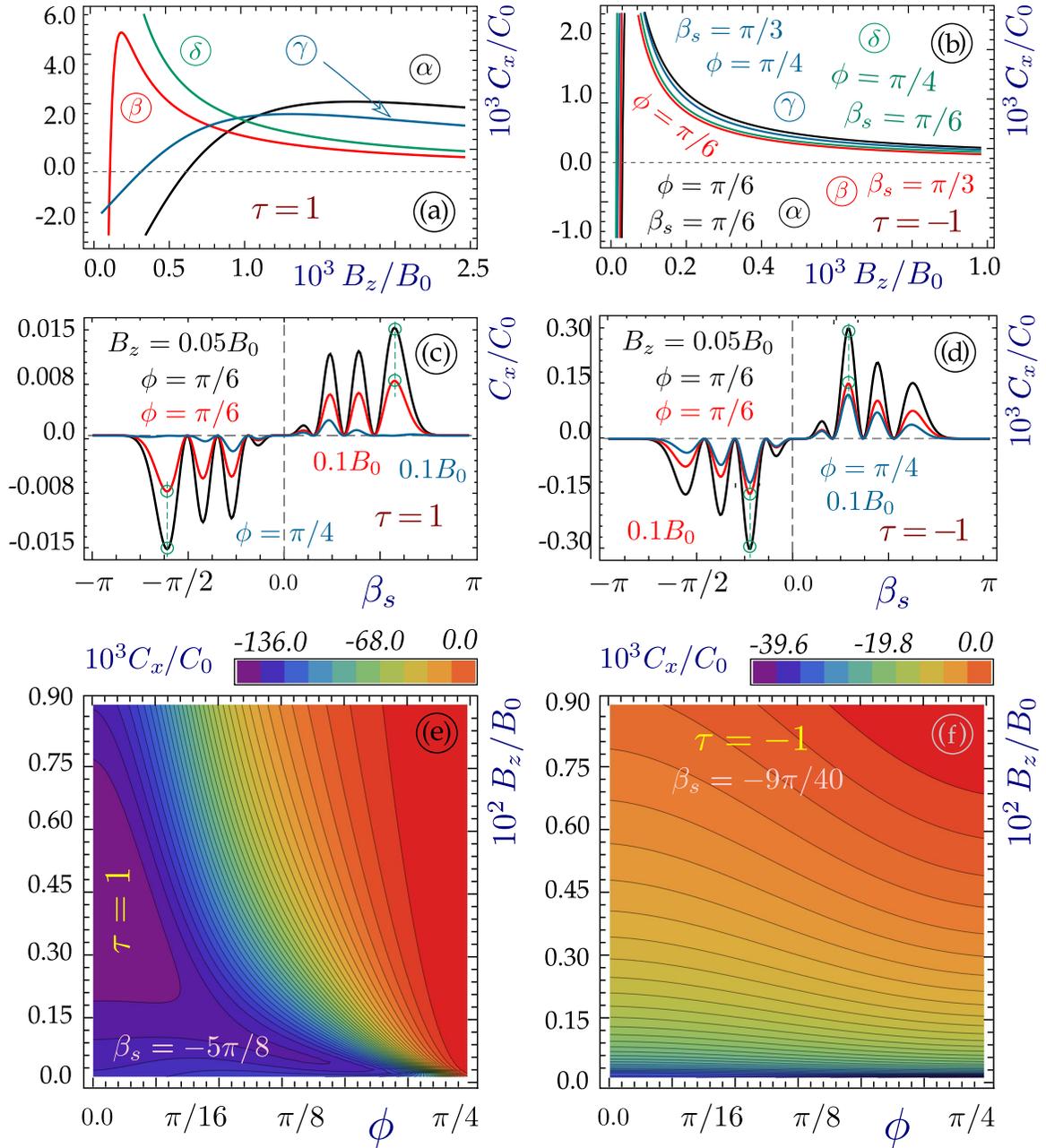
FIG. 7. (a)–(d) Back-scattering current-distribution component $C_x(k_F, \tau, \phi, \beta_s)$ from Eq. (19) as a function of B_z (a) and (b) with $\phi = \pi/4$, $\beta_s = \pi/6$ (green), $\phi = \pi/6$, $\beta_s = \pi/6$ (black), $\phi = \pi/4$, $\beta_s = \pi/3$ (blue), and $\phi = \pi/6$, $\beta_s = \pi/3$ (red) for $\tau = 1$ (a) and $\tau = -1$ (b), as well as a function of β_s with $\phi = \pi/6$, $B_z/B_0 = 0.05$ (black), $\phi = \pi/6$, $B_z/B_0 = 0.1$ (red), and $\phi = \pi/4$, $B_z/B_0 = 0.1$ (blue) for $\tau = 1$ (c) and $\tau = -1$ (d). 2D contour plots of $C_x(k_F, \tau, \phi, \beta_s)$ (e) and (f) as a function of both ϕ and B_z for $\beta_s = -5\pi/8$ and $\tau = 1$ (e) and for $\beta_s = -9\pi/40$ and $\tau = -1$ (f). Here two green circles in (c) and (d) indicate large back-scattering current peaks at $\beta_s \approx -5\pi/8$ ($\beta_s \approx -9\pi/40$) for $\tau = 1$ ($\tau = -1$), respectively. In addition, the unit of $C_0 = 4k_F v_F^2/\pi^2$ has been used for scaling $C_x(k_F, \tau, \phi, \beta_s)$ and B_0 is given in Fig. 5.

$C_y(k_F, \tau, \phi, \beta_s)$ as a function of both ϕ and B_z for $\tau = 1$ ($\tau = -1$) and $\beta_s = -3\pi/10$ ($\beta_s = -\pi/4$), respectively. We observe from Figs. 8(a) and 8(b) that for all cases $C_y(k_F, \tau, \phi, \beta_s)$ initially switches sign slow (fast) but subsequently decreases with B_z for $\tau = 1$ ($\tau = -1$), different from the results in Figs. 7(a) and 7(b). Increasing ϕ from $\pi/6$ (red) to $\pi/4$ (blue) at $\beta_s = \pi/3$ will reduce (enhance) $C_y(k_F, \tau, \phi, \beta_s)$ for $\tau = 1$ ($\tau = -1$) at very low B_z. However, $C_y(k_F, \tau, \phi, \beta_s)$ is always enhanced with ϕ for another scattering angle at $\beta_s = \pi/6$ with a bigger variation for $\tau =$

-1. From Figs. 8(c) and 8(d) we only see a strong (weak) sharp negative triplet skew-scattering peak in the full region of β_s with similar features as those found in Figs. 6(c) and 6(d) for their dependence on B_z and ϕ at $\tau = 1$ ($\tau = -1$). This leads to upward currents for both near-vertical (near-horizontal) forward and backward scattering at $\tau = 1$ ($\tau = -1$), respectively. The contour plot with $\beta_s = -3\pi/10$ and $\tau = 1$ in Fig. 8(e) again reveals a unique strong negative peak in $C_y(k_F, \tau, \phi, \beta_s)$ at the lower-right corner of this panel. For $\tau = -1$ and $\beta_s = -\pi/4$ in Fig. 8(f), on the other hand, only
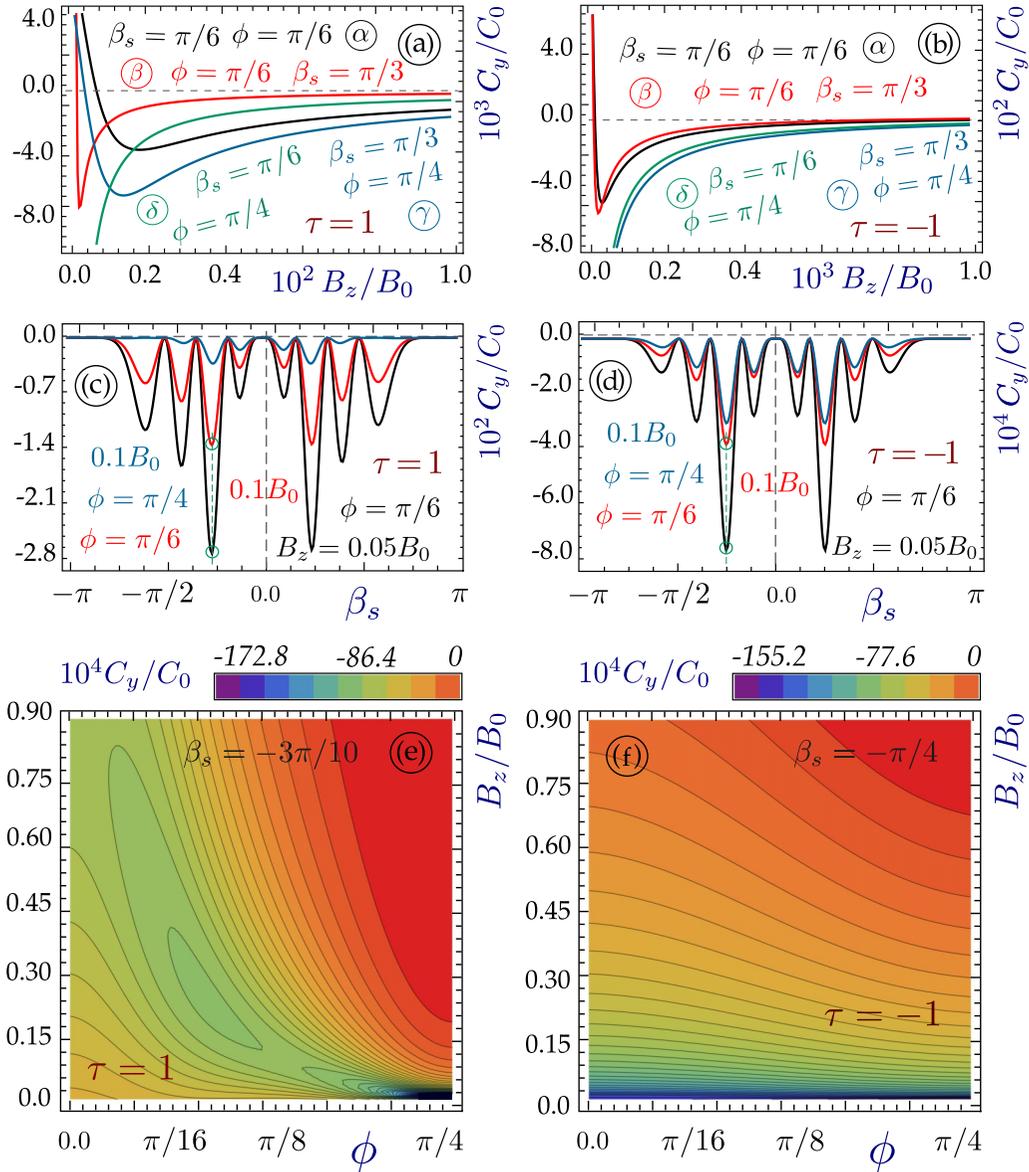
FIG. 8. (a)–(d) Skew-scattering current-distribution component $C_y(k_F, \tau, \phi, \beta_s)$ from Eq. (20) as a function of B_z (a) and (b) with $\phi = \pi/4$, $\beta_s = \pi/6$ (green), $\phi = \pi/6$, $\beta_s = \pi/6$ (black), $\phi = \pi/4$, $\beta_s = \pi/3$ (blue), and $\phi = \pi/6$, $\beta_s = \pi/3$ (red) for $\tau = 1$ (a) and $\tau = -1$ (b), as well as a function of β_s with $\phi = \pi/6$, $B_z/B_0 = 0.05$ (black), $\phi = \pi/6$, $B_z/B_0 = 0.1$ (red), and $\phi = \pi/4$, $B_z/B_0 = 0.1$ (blue) for $\tau = 1$ (c) and $\tau = -1$ (d). (e) and (f) 2D contour plots of $C_y(k_F, \tau, \phi, \beta_s)$ as a function of both ϕ and B_z for $\beta_s = -3\pi/10$ and $\tau = 1$ (e) and for $\beta_s = -\pi/4$ and $\tau = -1$ (f). Here two green circles in (c) and (d) indicate large skew-current peaks at $\beta_s \approx -3\pi/10$ ($\beta_s = -\pi/4$) for $\tau = 1$ ($\tau = -1$), respectively. In addition, C_0 and B_0 are given in Figs. 7 and 5, respectively.

one negative peak at bottom is seen for very small B_z, similar to that in Fig. 7(f).

For a comparison with experimentally measurable currents, we display in Fig. 9 the calculated total back-scattering current $j_{1x}(\tau, \phi)$ in Figs. 9(a) and 9(b), as well as total skew-scattering current $j_{1y}(\tau, \phi)$ in Figs. 9(c) and 9(d), from Eq. (11) as a function of B_z with various phases ϕ for $\tau = 1$ [Figs. 9(a) and 9(c)] and $\tau = -1$ [Figs. 9(b) and 9(d)]. From Figs. 9(a) and 9(b) we see a slow (fast) monotonic decrease of $j_{1x}(\tau, \phi)$ with increasing B_z in the scale of $\sim 1/B_z^2$ for $\tau = 1$ ($\tau = -1$) due to cyclotron motion. Such different behaviors are attributed to lower (higher) mobility at the $\tau = 1$ ($\tau = -1$) valley. However, increasing ϕ reduces $j_{1x}(\tau, \phi)$ for

both $\tau = \pm 1$, similar to the observed behaviors in Figs. 5(a) and 5(b). For $j_{1y}(\tau, \phi)$ in Figs. 9(c) and 9(d), on the other hand, the same Lorentz force initially strengthens $j_{1y}(\tau, \phi)$ dramatically for all values of ϕ and $\tau = \pm 1$ at very low B_z but eventually weakens $j_{1y}(\tau, \phi)$ slowly (quickly) for $\tau = 1$ ($\tau = -1$) in the strong-field limit (in the scale of $\sim 1/B_z$) due to cyclotron motion of electrons. Such a huge initial increase in $j_{1y}(\tau, \phi)$ at very low B_z is greatly suppressed in graphene with the maximum Berry force at $\phi = 0$ (black). Consequently, a Berry-phase dependent asymmetry in suppressing the skew currents by electron cyclotron motion can be seen by directly comparing Fig. 9(c) with Fig. 9(d). For a gVHE, the Berry phase can be used for mediating the VHE. In our case, an
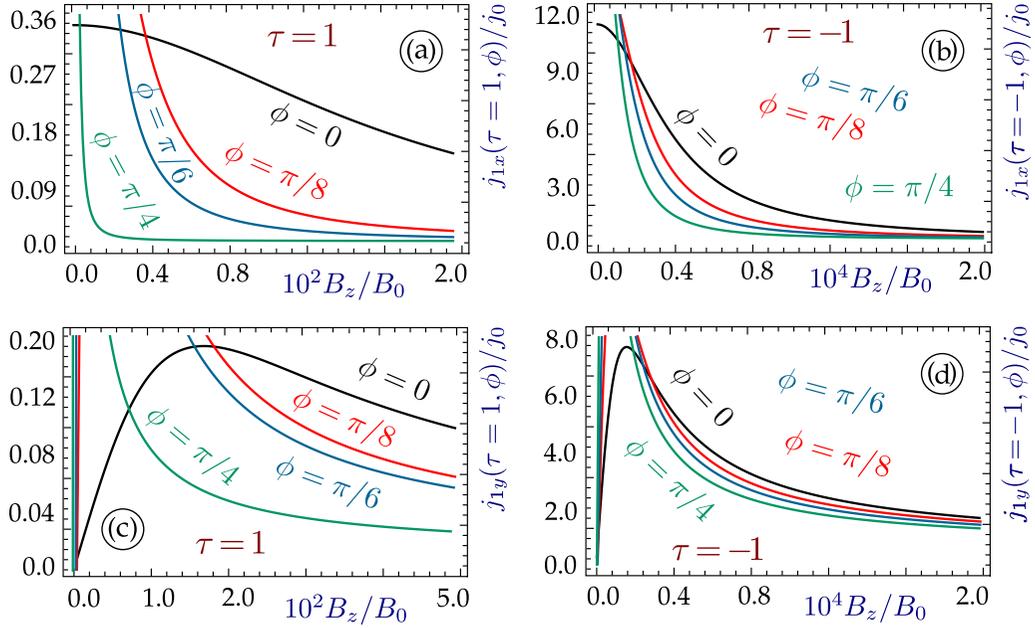
FIG. 9. Calculated nonequilibrium total back-scattering current $j_{1x}(\tau, \phi)$ (a) and (b) and total skew-scattering current $j_{1y}(\tau, \phi)$ (c) and (d) from Eq. (11) as a function of B_z with $\phi = \pi/4$ (green), $\phi = \pi/6$ (blue), $\phi = \pi/8$ (red), and $\phi = 0$ (black) for $\tau = 1$ (a) and (c) and $\tau = -1$ (b) and (d). Here B_0 and j_0 are given in Figs. 5 and 6, respectively.

external magnetic field can be employed further to control this gVHE. Experimentally, one can directly measure both the back-scatter and the skew-scattering nonequilibrium electrical currents calculated by Eq. (11) as a function of perpendicular magnetic field B_z using the standard van der Pauw method [43] so as to verify unique features associated with different geometry phases ϕ at low B_z, including graphene and dice lat-

tice. In this case, however, the contributions from equilibrium longitudinal and Hall currents in Fig. 10 (see discussions of Fig. 10 below) should be deducted from the corresponding total current measured.

Finally, from Eq. (12) we know there exists another conduction current $\boldsymbol{j}_2(\tau, \phi)$ even in the thermal-equilibrium state due to Berry curvature $\boldsymbol{\Omega}_\perp(\boldsymbol{k}_\parallel)$, leading to the
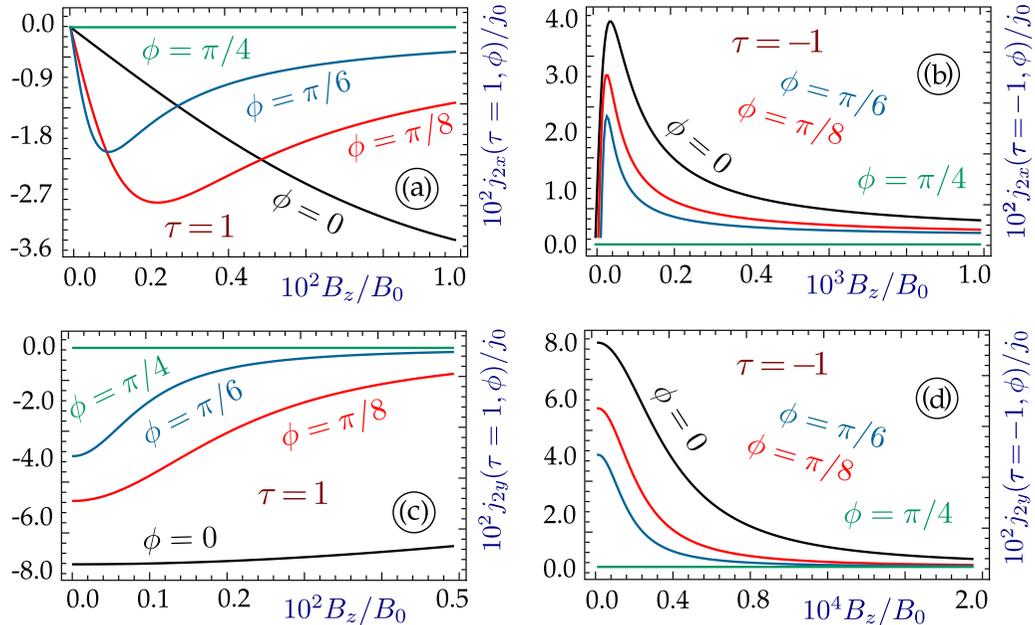
FIG. 10. Calculated thermal-equilibrium Berry-curvature induced longitudinal current $j_{2x}(\tau, \phi)$ (a) and (b) and Hall current $j_{2y}(\tau, \phi)$ (c) and (d) from Eq. (12) as a function of B_z with $\phi = \pi/4$ (green), $\phi = \pi/6$ (blue), $\phi = \pi/8$ (red), and $\phi = 0$ (black) for $\tau = 1$ (a) and (c) and $\tau = -1$ (b) and (d). Here B_0 and j_0 are given in Figs. 5 and 6, respectively.

so-called anomalous Hall effect (AHE) if $\phi \neq \pi/4$. Figure 10 presents the calculated AHE current components $j_{2x}(\tau, \phi)$ in Figs. 10(a) and 10(b) and $j_{2y}(\tau, \phi)$ in Figs. 10(c) and 10(d). Since $\boldsymbol{j}_2(\tau, \phi)$ is proportional to τ (i.e., valley dependent), we expect the opposite signs in Figs. 10(a) and 10(b) for $j_{2x}(\tau, \phi)$ and in Figs. 10(c) and 10(d) for $j_{2y}(\tau, \phi)$. As an indication of gVHE, the increase of the Berry force (or reducing ϕ) in momentum space will slowly (quickly) enlarge $j_{2x}(\tau, \phi)$ at small B_z and $j_{2y}(\tau, \phi)$ at $B_z = 0$ simultaneously due to large (small) mobility at $\tau = 1$ ($\tau = -1$). However, this AHE current is always weakened by the Lorentz force (or increasing B_z) in position space for large B_z, where $j_{2x}(\tau, \phi)$ is induced only by one term $\sim B_z \mu_{xx} E_x$, while $j_{2y}(\tau, \phi)$ is generated by two terms $\sim (1 + B_z \mu_{yx}) E_x$. Therefore, $j_{2x}(\tau, \phi)$ decreases like $\sim 1/B_z$ in the high-field limit. Meanwhile, $j_{2y}(\tau, \phi)$ also approaches zero in the same strong-field limit but it scales as $\sim 1/B_z^2$. Since there are two orders of magnitude difference in μ_{xx} and μ_{yx} for $\tau = 1$ and -1, we expect the decrease in $j_{2x}(\tau, \phi)$ and $j_{2y}(\tau, \phi)$ to become much faster at the $\tau = -1$ valley, and therefore a net AHE current (sum of currents from both valleys) exists and will be dominated by the $\tau = 1$ valley for large B_z. We can make use of the experimentally measured mobility tensor and Eq. (12) to independently quantify the Berry-curvature induced longitudinal and Hall currents as a function of perpendicular magnetic field B_z.

triplet peak at two distinct valleys and in near-horizontal and near-vertical scattering directions for forward- and back-scattering current, which favor small Berry phases and low magnetic fields. We also show a magnetic-field dependence of both nonequilibrium and thermal-equilibrium conduction currents from Berry-phase-mediated and valley-dependent longitudinal and transverse transport.

In our theory we have employed the first two Boltzmann moment equations in calculations of scattering-angle distributions for extrinsic skew-scattering currents due to the presence of random impurities in α-T_3 lattices, where both energy- and momentum-relaxation times are computed microscopically. We attribute this scattering-angle dependence to an anisotropic inverse momentum-relaxation-time tensor calculated within the screened second-order Born approximation and using a static dielectric function within the random-phase approximation. Meanwhile, we also include the isotropic intrinsic current due to Berry curvature for electrons in thermal-equilibrium states. Under a perpendicular non-quantizing magnetic field, we find an interplay by Lorentz and valley-dependent resistive forces acting on electrons, leading to field-dependent skew currents. We further find these skew currents can be mediated by Berry phases of α-T_3 lattices and depend on barrier- or trap-type impurity potentials at two inequivalent valleys.

IV. CONCLUSIONS AND REMARKS

In conclusion, we have demonstrated the Berry-phase mediation to valley-dependent Hall transport in α-T_3 lattices. We analyze and explain the found interplay between the Lorentz force in position space and the Berry force in momentum space for the total sheet current density including both normal conduction and Hall currents as well as anomalous Hall current. We also include many-body screening effects on electron-impurity interactions, which is crucial for avoiding overestimation of elastic scattering. We further find

ACKNOWLEDGMENTS

APPENDIX A: IMPURITY SCATTERING MATRIX

For impurity scattering of electrons in an α-T_3 lattice, the initial $|i\rangle$ and final $|f\rangle$ states for Bloch electrons with wave vectors $\boldsymbol{k}_\parallel$ and $\boldsymbol{k}'_\parallel$ can be written as $|i\rangle = \frac{e^{i\mathbf{k}_\parallel \cdot \mathbf{r}_\parallel}}{\sqrt{S}} |s, \tau, \boldsymbol{k}_\parallel\rangle_\phi$ and $|f\rangle = \frac{e^{i\mathbf{k}'_\parallel \cdot \mathbf{r}_\parallel}}{\sqrt{S}} |s, \tau, \boldsymbol{k}'_\parallel\rangle_\phi$, where $|s, \tau, \boldsymbol{k}_\parallel\rangle_\phi$ is given by Eq. (2) and S is the sheet area. We assume an isotropic sublattice-selected steplike impurity-scattering potential, i.e., $u_0^\tau(r_\parallel) = \tau V_0 \Theta(r_0 - r_\parallel)$, for electrons, where V_0 is the step height, r_0 represents the interaction range, and $\tau = +1$ (or $\tau = -1$) corresponds to a barrierlike (or traplike) impurity potential. As a result, the screened impurity scattering matrix is found to be [44]

$$
\begin{aligned}
U_{\text{im}}^{\tau, \phi}(\boldsymbol{k}'_\parallel, \boldsymbol{k}_\parallel) &= \sum_{\mathbf{q}'_\parallel} \frac{U_0^\tau(q'_\parallel)}{\epsilon_\phi(q'_\parallel)} \langle f | e^{i\mathbf{q}'_\parallel \cdot \mathbf{r}_\parallel} | i \rangle = \sum_{\mathbf{q}'_\parallel} \frac{U_0^\tau(q'_\parallel)}{\epsilon_\phi(q'_\parallel)} \\
&\times \sum_\ell \langle f | \ell \rangle_{\tau, \phi\ \tau, \phi} \langle \ell | e^{i\mathbf{q}'_\parallel \cdot \mathbf{r}_\parallel} | i \rangle = \frac{1}{2S} \sum_{\mathbf{q}'_\parallel} \frac{U_0^\tau(q'_\parallel)}{\epsilon_\phi(q'_\parallel)} \sum_\ell \int_{r'_\parallel \leqslant r_0} d^2 \boldsymbol{r}'_\parallel\, e^{-i\mathbf{k}'_\parallel \cdot \mathbf{r}'_\parallel} \frac{e^{i\ell \Theta_{\mathbf{r}'_\parallel}}}{\sqrt{2\pi}} \\
&\times \left\{ \tau \cos\phi\, e^{-i\tau(\Theta_{\mathbf{r}'_\parallel} - \theta_{\mathbf{k}'_\parallel})} \mathcal{R}_1(r'_\parallel) + s \mathcal{R}_2(r'_\parallel) + \tau \sin\phi\, e^{i\tau(\Theta_{\mathbf{r}'_\parallel} - \theta_{\mathbf{k}'_\parallel})} \mathcal{R}_3(r'_\parallel) \right\} \int_{r_\parallel \leqslant r_0} d^2 \boldsymbol{r}_\parallel\, e^{i(\mathbf{q}'_\parallel + \mathbf{k}_\parallel) \cdot \mathbf{r}_\parallel} \\
&\times \frac{e^{-i\ell \Theta_{\mathbf{r}_\parallel}}}{\sqrt{2\pi}} \left\{ \tau \cos\phi\, e^{i\tau(\Theta_{\mathbf{r}_\parallel} - \theta_{\mathbf{k}_\parallel})} \mathcal{R}_1^*(r_\parallel) + s \mathcal{R}_2^*(r_\parallel) + \tau \sin\phi\, e^{-i\tau(\Theta_{\mathbf{r}_\parallel} - \theta_{\mathbf{k}_\parallel})} \mathcal{R}_3^*(r_\parallel) \right\},
\end{aligned} \tag{A1}
$$

where $U_0(q'_\parallel)/\epsilon_\phi(q'_\parallel)$ is the 2D Fourier transform of the screened impurity potential, and

$$|\ell\rangle_{\tau,\phi} = \frac{e^{i\ell\Theta_{\mathbf{r}_\parallel}}}{\sqrt{2\pi}} \begin{bmatrix} \mathcal{R}_1(r_\parallel)\,e^{-i\tau\Theta_{\mathbf{r}_\parallel}} \\ \mathcal{R}_2(r_\parallel) \\ \mathcal{R}_3(r_\parallel)\,e^{i\tau\Theta_{\mathbf{r}_\parallel}} \end{bmatrix}$$

are the intermediate quantum states for scattered electrons by an ionized impurity atom with a locally spherical symmetry [see Eq. (C7) below] at the valley $|\tau\rangle$. Moreover, the first integral with respect to $\mathbf{r}'_\parallel$ in Eq. (A1) can be evaluated analytically and gives rise to

$$
\begin{aligned}
\text{Integral-}\mathbf{r}'_\parallel &= \int_0^{r_0} dr'_\parallel\, r'_\parallel \int_0^{2\pi} d\Theta_{\mathbf{r}'_\parallel} \frac{e^{i\ell\Theta_{\mathbf{r}'_\parallel}}}{\sqrt{2\pi}} \sum_m J_m(k'_\parallel r'_\parallel)\, e^{-im(\theta_{\mathbf{k}'_\parallel} - \Theta_{\mathbf{r}'_\parallel})}\, (-i)^m \\
&\quad \times \left\{ \tau\cos\phi\, e^{-i\tau(\Theta_{\mathbf{r}'_\parallel} - \theta_{\mathbf{k}'_\parallel})} \mathcal{R}_1(r'_\parallel) + s\mathcal{R}_2(r'_\parallel) + \tau\sin\phi\, e^{i\tau(\Theta_{\mathbf{r}'_\parallel} - \theta_{\mathbf{k}'_\parallel})} \mathcal{R}_3(r'_\parallel) \right\} \\
&= \sqrt{2\pi}(-i)^\ell\, e^{i\ell\theta_{\mathbf{k}'_\parallel}} \int_0^{r_0} dr'_\parallel\, r'_\parallel [(-i)^{-\tau}\, \tau\cos\phi\, J_{\ell-\tau}(k'_\parallel r'_\parallel)\, \mathcal{R}_1(r'_\parallel) \\
&\quad + sJ_\ell(k'_\parallel r'_\parallel)\, \mathcal{R}_2(r'_\parallel) + (-i)^\tau\, \tau\sin\phi\, J_{\ell+\tau}(k'_\parallel r'_\parallel)\, \mathcal{R}_3(r'_\parallel)].
\end{aligned}
$$

Similarly, for the second integral with respect to $\mathbf{r}_\parallel$ in Eq. (A1), we have

$$
\begin{aligned}
\text{Integral-}\mathbf{r}_\parallel &= \int_0^{r_0} dr_\parallel\, r_\parallel \int_0^{2\pi} d\Theta_{\mathbf{r}_\parallel} \frac{e^{-i\ell\Theta_{\mathbf{r}_\parallel}}}{\sqrt{2\pi}} \sum_m J_m(|\mathbf{k}_\parallel + \mathbf{q}'_\parallel| r_\parallel)\, e^{im(\theta_{\mathbf{k}_\parallel + \mathbf{q}'_\parallel} - \Theta_{\mathbf{r}_\parallel})}\, (i)^m \\
&\quad \times \left\{ \tau\cos\phi\, e^{i\tau(\Theta_{\mathbf{r}_\parallel} - \theta_{\mathbf{k}_\parallel})} \mathcal{R}_1^*(r_\parallel) + s\mathcal{R}_2^*(r_\parallel) + \tau\sin\phi\, e^{-i\tau(\Theta_{\mathbf{r}_\parallel} - \theta_{\mathbf{k}_\parallel})} \mathcal{R}_3^*(r_\parallel) \right\} \\
&= \sqrt{2\pi}\,(i)^\ell\, e^{-i\ell\theta_{\mathbf{k}_\parallel + \mathbf{q}'_\parallel}} \int_0^{r_0} dr_\parallel\, r_\parallel \left\{ (-i)^\tau\, \tau\cos\phi\, J_{\ell-\tau}(|\mathbf{k}_\parallel + \mathbf{q}'_\parallel| r_\parallel)\, \mathcal{R}_1^*(r_\parallel)\, e^{i\tau\beta^s_{\mathbf{k}_\parallel,\mathbf{q}'_\parallel}} \right. \\
&\quad \left. + sJ_\ell(|\mathbf{k}_\parallel + \mathbf{q}'_\parallel| r_\parallel)\, \mathcal{R}_2^*(r_\parallel) + (-i)^{-\tau}\, \tau\sin\phi\, J_{\ell+\tau}(|\mathbf{k}_\parallel + \mathbf{q}'_\parallel| r_\parallel)\, \mathcal{R}_3^*(r_\parallel)\, e^{-i\tau\beta^s_{\mathbf{k}_\parallel,\mathbf{q}'_\parallel}} \right\},
\end{aligned}
$$

where $\beta^s_{\mathbf{k}_\parallel,\mathbf{q}'_\parallel} = \theta_{\mathbf{k}_\parallel + \mathbf{q}'_\parallel} - \theta_{\mathbf{k}_\parallel}$ is the scattering angle. Finally, by combining the results for these two integrals and inserting them into Eq. (A1) we obtain a simple expression

$$U_{\text{im}}^{\tau,\phi}(\mathbf{k}_\parallel + \mathbf{q}_\parallel, \mathbf{k}_\parallel) = \frac{U_0^\tau(q_\parallel)}{\epsilon_\phi(q_\parallel)\mathcal{S}} \mathcal{F}_{\tau,\phi}(\mathbf{k}_\parallel, \mathbf{q}_\parallel), \tag{A2}$$

where the form factor $\mathcal{F}_{\tau,\phi}(\mathbf{k}_\parallel, \mathbf{q}_\parallel)$ is defined as

$$
\begin{aligned}
\mathcal{F}_{\tau,\phi}(\mathbf{k}_\parallel, \mathbf{q}_\parallel) &= \frac{1}{2} \sum_\ell \{ (-i)^{-\tau}\, \tau\cos\phi\, \chi_1(|\mathbf{k}_\parallel + \mathbf{q}_\parallel|) + s\chi_2(|\mathbf{k}_\parallel + \mathbf{q}_\parallel|) + (-i)^\tau\, \tau\sin\phi\, \chi_3(|\mathbf{k}_\parallel + \mathbf{q}_\parallel|) \} \\
&\quad \times \left\{ (-i)^\tau\, \tau\cos\phi\, \chi_1^*(|\mathbf{k}_\parallel + \mathbf{q}_\parallel|)\, e^{i\tau\beta^s_{\mathbf{k}_\parallel,\mathbf{q}_\parallel}} + s\chi_2^*(|\mathbf{k}_\parallel + \mathbf{q}_\parallel|) + (-i)^{-\tau}\, \tau\sin\phi\, \chi_3^*(|\mathbf{k}_\parallel + \mathbf{q}_\parallel|)\, e^{-i\tau\beta^s_{\mathbf{k}_\parallel,\mathbf{q}_\parallel}} \right\}. \quad \text{(A3)}
\end{aligned}
$$

Furthermore, we have introduced the notations in Eq. (A3), given by

$$\begin{Bmatrix} \chi_1(|\mathbf{k}_\parallel + \mathbf{q}_\parallel|) \\ \chi_2(|\mathbf{k}_\parallel + \mathbf{q}_\parallel|) \\ \chi_3(|\mathbf{k}_\parallel + \mathbf{q}_\parallel|) \end{Bmatrix} = \sqrt{2\pi} \int_0^{r_0} dr_\parallel\, r_\parallel \begin{Bmatrix} J_{\ell-\tau}(|\mathbf{k}_\parallel + \mathbf{q}_\parallel| r_\parallel)\, \mathcal{R}_1(r_\parallel) \\ J_\ell(|\mathbf{k}_\parallel + \mathbf{q}_\parallel| r_\parallel)\, \mathcal{R}_2(r_\parallel) \\ J_{\ell+\tau}(|\mathbf{k}_\parallel + \mathbf{q}_\parallel| r_\parallel)\, \mathcal{R}_3(r_\parallel) \end{Bmatrix}, \tag{A4}$$

where a wave-function normalization factor should be included as shown in Eq. (C6).

APPENDIX B: DIELECTRIC FUNCTION

Under the random-phase approximation [45], the dielectric function $\epsilon_\phi(q_\parallel, \omega)$ for α-T_3 lattices is calculated as

$$\epsilon_\phi(q_\parallel, \omega) = 1 + \left(\frac{e^2}{2\epsilon_0\epsilon_r q_\parallel} \right) \mathcal{Q}_\phi(q_\parallel, \omega), \tag{B1}$$

where the polarization function $\mathcal{Q}_\phi(q_\parallel, \omega)$ is given by

$$\mathcal{Q}_\phi(q_\parallel, \omega) = \frac{2}{\mathcal{S}} \sum_{\tau,\mathbf{k}_\parallel,s,s'} \mathcal{G}_{s,s'}^{\tau,\phi}(\mathbf{k}_\parallel, \mathbf{q}_\parallel) \left\{ \frac{f_T^{(0)}[\varepsilon_{s'}(|\mathbf{k}_\parallel + \mathbf{q}_\parallel|)] - f_T^{(0)}[\varepsilon_s(k_\parallel)]}{\hbar(\omega + i0^+) - \varepsilon_{s'}(|\mathbf{k}_\parallel + \mathbf{q}_\parallel|) + \varepsilon_s(k_\parallel)} \right\}. \tag{B2}$$

Here the prefactor 2 comes from the spin degeneracy, $\mathcal{S}$ is the sheet area, $\varepsilon_s(k_\parallel) = s\hbar v_F k_\parallel$ for $s = 0, \pm 1$, ω is the angular frequency of a probe field, $f_T^{(0)}(x) = \{1 + \exp[(x - u_0)/k_B T]\}^{-1}$ is the Fermi function for electrons in thermal-equilibrium states, $u_0(T)$ is the chemical potential for doped electrons, and T is the temperature. In addition, the overlap integral $\mathcal{G}_{s,s'}^{\tau,\phi}(k_\parallel, q_\parallel)$ introduced in Eq. (B2) is defined by

$$\mathcal{G}_{s,s'}^{\tau,\phi}(k_\parallel, q_\parallel) = \mathcal{G}_{s',s}^{\tau,\phi}(q_\parallel, k_\parallel) = |_\phi\langle s, \tau, k_\parallel | s', \tau, k_\parallel + q_\parallel \rangle_\phi|^2, \tag{B3}$$

and the wave functions $|s, \tau, k_\parallel\rangle_\phi$ for $s = 0, \pm 1$ and $\tau = \pm 1$ are given by Eqs. (2) and (3). At low T, the remaining nonzero terms in Eq. (B2) in the summation over s and s' correspond to $s' = +1$, $s = 0, \pm 1$, or vice versa. Therefore, we get three finite terms [20] from Eq. (B3):

$$\mathcal{G}_{0,+1}^{\tau,\phi}(k_\parallel, q_\parallel) = \tfrac{1}{2} \sin^2(2\phi) \sin^2\left(\beta_{\mathbf{k}_\parallel,\mathbf{q}_\parallel}^s\right), \tag{B4}$$

$$\mathcal{G}_{\pm 1,+1}^{\tau,\phi}(k_\parallel, q_\parallel) = \tfrac{1}{4}\left\{1 \pm \cos\left(\beta_{\mathbf{k}_\parallel,\mathbf{q}_\parallel}^s\right)\right\}^2 + \tfrac{1}{4} \cos^2(2\phi) \sin^2\left(\beta_{\mathbf{k}_\parallel,\mathbf{q}_\parallel}^s\right), \tag{B5}$$

which are independent of $\tau = \pm 1$, where $\beta_{\mathbf{k}_\parallel,\mathbf{q}_\parallel}^s = \theta_{\mathbf{k}_\parallel+\mathbf{q}_\parallel} - \theta_{\mathbf{k}_\parallel}$ is the angle between two wave vectors $k_\parallel$ and $k_\parallel + q_\parallel$, and $\theta_{\mathbf{k}_\parallel} = \tan^{-1}(k_y/k_x)$ is the angle between $k_\parallel$ and x axis.

After setting $\omega = 0$, we obtain the static dielectric function $\epsilon_\phi(q_\parallel)$ from Eq. (B1) using

$$\mathcal{Q}_\phi(q_\parallel, \omega = 0) = a_\phi(q_\parallel) + \Theta(q_\parallel - 2k_F) b_\phi(q_\parallel), \tag{B6}$$

where $k_F = \sqrt{\pi \rho_0}$, and ρ_0 is the areal density of doped electrons. If $q_\parallel < 2k_F$ is further assumed, we find $q_\phi = (e^2/2\epsilon_0\epsilon_r) a_\phi(q_\parallel) \approx (e^2 k_F)/(\pi \epsilon_0 \epsilon_r \hbar v_F)$ for $\epsilon_\phi(q_\parallel) = 1 + q_\phi/q_\parallel$. As $q_\parallel \ll k_F$, $a_\phi(q_\parallel)$ becomes independent of ϕ and is given by [20]

$$a_\phi(q_\parallel) = \frac{1}{2\pi \hbar v_F}\left(4k_F + \frac{q_\parallel^2}{k_F}\right) \approx \frac{2k_F}{\pi \hbar v_F}. \tag{B7}$$

APPENDIX C: ENERGY-RELAXATION TIME

By using the detailed-balance condition, the microscopic energy-relaxation time $\tau_\phi(k_\parallel, \tau)$ introduced in Eq. (7) can be calculated according to [41]

$$\frac{1}{\tau_\phi(k_\parallel, \tau)} = \mathcal{W}_{\text{in}}^{\tau,\phi}(k_\parallel) + \mathcal{W}_{\text{out}}^{\tau,\phi}(k_\parallel), \tag{C1}$$

where the scattering-in rate for electrons in the final $k_\parallel$ state is

$$\mathcal{W}_{\text{in}}^{\tau,\phi}(k_\parallel) = \frac{\pi N_i}{\hbar} \sum_{\mathbf{q}_\parallel} \left|U_{\text{im}}^{\tau,\phi}(q_\parallel, k_\parallel)\right|^2 \{f_{\mathbf{k}_\parallel-\mathbf{q}_\parallel} \delta(\varepsilon_{\mathbf{k}_\parallel} - \varepsilon_{\mathbf{k}_\parallel-\mathbf{q}_\parallel}) + f_{\mathbf{k}_\parallel+\mathbf{q}_\parallel} \delta(\varepsilon_{\mathbf{k}_\parallel} - \varepsilon_{\mathbf{k}_\parallel+\mathbf{q}_\parallel})\}, \tag{C2}$$

and the scattering-out rate for electrons in the initial $k_\parallel$ state is

$$\mathcal{W}_{\text{out}}^{\tau,\phi}(k_\parallel) = \frac{\pi N_i}{\hbar} \sum_{\mathbf{q}_\parallel} \left|U_{\text{im}}^{\tau,\phi}(q_\parallel, k_\parallel)\right|^2 \{(1 - f_{\mathbf{k}_\parallel+\mathbf{q}_\parallel}) \delta(\varepsilon_{\mathbf{k}_\parallel+\mathbf{q}_\parallel} - \varepsilon_{\mathbf{k}_\parallel}) + (1 - f_{\mathbf{k}_\parallel-\mathbf{q}_\parallel}) \delta(\varepsilon_{\mathbf{k}_\parallel-\mathbf{q}_\parallel} - \varepsilon_{\mathbf{k}_\parallel})\}. \tag{C3}$$

Here, for simplicity, we have introduced the notations $f_{\mathbf{k}_\parallel} \equiv f_T^{(0)}[\varepsilon(k_\parallel)]$ and $\varepsilon_{\mathbf{k}_\parallel} \equiv \varepsilon_+(k_\parallel)$. We have also assumed low T and ρ_0 so that both phonon and pair scattering can be neglected in comparison with dominant impurity scattering. In addition, N_i represents the number of randomly distributed ionized impurities in the system, and $|U_{\text{im}}^{\tau,\phi}(q_\parallel, k_\parallel)|^2$ comes from the random-impurity scattering within the second-order Born approximation.

Explicitly, using the results in Appendix A, we write down the expression for the screened impurity scattering interaction as

$$\left|U_{\text{im}}^{\tau,\phi}(q_\parallel, k_\parallel)\right|^2 = \left|\frac{U_0^\tau(q_\parallel)}{\epsilon_\phi(q_\parallel) \mathcal{S}}\right|^2 |\mathcal{F}_{\tau,\phi}(k_\parallel, q_\parallel)|^2, \tag{C4}$$

where $\mathcal{S}$ is the sheet area, and $\epsilon_\phi(q_\parallel)$ is a static dielectric function [see Eqs. (B1) and (B6)]. In addition, the scattering form factor $\mathcal{F}_{\tau,\phi}(\mathbf{k}_\parallel, \mathbf{q}_\parallel)$ in Eq. (C4) is given by

$$\mathcal{F}_{\tau,\phi}(k_\parallel, q_\parallel) = \frac{1}{2} \sum_\ell \{(-i)^{-\tau} \tau \cos\phi \, \chi_1(|k_\parallel + q_\parallel|) + s\chi_2(|k_\parallel + q_\parallel|) + (-i)^\tau \tau \sin\phi \, \chi_3(|k_\parallel + q_\parallel|)\}$$

$$\times \{(-i)^\tau \tau \cos\phi \, \chi_1^*(|k_\parallel + q_\parallel|) e^{i\tau \beta_{\mathbf{k}_\parallel,\mathbf{q}_\parallel}^s} + s\chi_2^*(|k_\parallel + q_\parallel|) + (-i)^{-\tau} \tau \sin\phi \, \chi_3^*(|k_\parallel + q_\parallel|) e^{-i\tau \beta_{\mathbf{k}_\parallel,\mathbf{q}_\parallel}^s}\}. \tag{C5}$$

where $s = +1$ is selected for doped electrons, $\tau = \pm 1$ for two inequivalent valleys, $\alpha = \tan\phi$ is the parameter identifying nonequivalent crystalline sublattices, $\beta^s_{\mathbf{k}_\parallel,\mathbf{q}_\parallel} \equiv \theta_{\mathbf{k}_\parallel+\mathbf{q}_\parallel} - \theta_{\mathbf{k}_\parallel}$ is the scattering angle, $\theta_{\mathbf{k}_\parallel} = \tan^{-1}(k_y/k_x)$, and $\theta_{\mathbf{k}_\parallel+\mathbf{q}_\parallel} = \tan^{-1}[(k_y + q_y)/(k_x + q_x)]$. Furthermore, we define the scattering factors in Eq. (C5) by

$$
\frac{1}{\sqrt{2\pi}}
\begin{Bmatrix}
\chi_1(|\mathbf{k}_\parallel + \mathbf{q}_\parallel|) \\
\chi_2(|\mathbf{k}_\parallel + \mathbf{q}_\parallel|) \\
\chi_3(|\mathbf{k}_\parallel + \mathbf{q}_\parallel|)
\end{Bmatrix}
= \left\{ \int_0^1 d\xi\, \xi (|\mathcal{R}_1(\xi)|^2 + |\mathcal{R}_2(\xi)|^2 + |\mathcal{R}_3(\xi)|^2) \right\}^{-1/2}
\int_0^1 d\xi\, \xi
\begin{Bmatrix}
J_{\ell-\tau}(|\mathbf{k}_\parallel + \mathbf{q}_\parallel|r_0\xi)\,\mathcal{R}_1(\xi) \\
J_\ell(|\mathbf{k}_\parallel + \mathbf{q}_\parallel|r_0\xi)\,\mathcal{R}_2(\xi) \\
J_{\ell+\tau}(|\mathbf{k}_\parallel + \mathbf{q}_\parallel|r_0\xi)\,\mathcal{R}_3(\xi)
\end{Bmatrix},
\quad \text{(C6)}
$$

where $J_\ell(x)$ is the Bessel function of the first kind, ℓ is the angular-momentum quantum number, and r_0 is the range of impurity interaction. In addition, the radial parts of the wave function $\mathcal{R}_1(\xi)$, $\mathcal{R}_2(\xi)$, and $\mathcal{R}_3(\xi)$, introduced in Eq. (C6), satisfy the following matrix-form Dirac equation for massless three-component generalization of Dirac-Weyl particles [31]

$$
\begin{bmatrix}
u_0^\tau(\xi) & -\frac{i\tau\hbar v_F \cos\phi}{r_0}\left(\frac{d}{d\xi} + \frac{\tau\ell}{\xi}\right) & 0 \\
-\frac{i\tau\hbar v_F \cos\phi}{r_0}\left(\frac{d}{d\xi} - \frac{\tau(\ell-\tau)}{\xi}\right) & u_0^\tau(\xi) & -\frac{i\tau\hbar v_F \sin\phi}{r_0}\left(\frac{d}{d\xi} + \frac{\tau(\ell+\tau)}{\xi}\right) \\
0 & -\frac{i\tau\hbar v_F \sin\phi}{r_0}\left(\frac{d}{d\xi} - \frac{\tau\ell}{\xi}\right) & u_0^\tau(\xi)
\end{bmatrix}
\otimes
\begin{bmatrix}
\mathcal{R}_1(\xi) \\
\mathcal{R}_2(\xi) \\
\mathcal{R}_3(\xi)
\end{bmatrix}
= E_0(k_\parallel)
\begin{bmatrix}
\mathcal{R}_1(\xi) \\
\mathcal{R}_2(\xi) \\
\mathcal{R}_3(\xi)
\end{bmatrix},
\quad \text{(C7)}
$$

where $E_0(k_\parallel)$ represents the given kinetic energy of incident electrons, $u_0^\tau(\xi) = \tau V_0\,\Theta(1-\xi)$ for a barrierlike ($\tau = +1$) or a traplike ($\tau = -1$) impurity potential, V_0 is a potential-step height in the region of $0 \leqslant \xi = r/r_0 \leqslant 1$, and

$$
U_0^\tau(q_\parallel) = \tau V_0 (2\pi r_0^2) \int_0^1 d\xi\, \xi J_0(\xi r_0 q_\parallel)
\quad \text{(C8)}
$$

is the Fourier transform of the scattering potential $u_0^\tau(\xi)$. It is clear from Eqs. (C5)–(C7) that $\mathcal{F}_{\tau,\phi}(\mathbf{k}_\parallel,\mathbf{q}_\parallel) \neq \mathcal{F}_{-\tau,\phi}(\mathbf{k}_\parallel,\mathbf{q}_\parallel)$ and $\chi_1(|\mathbf{k}_\parallel + \mathbf{q}_\parallel|) \neq \chi_3(|\mathbf{k}_\parallel + \mathbf{q}_\parallel|)$ if $\phi \neq \pi/4$, which gives rise to valley-dependent impurity scattering. This can be attributed to the change from the translational symmetry in a crystal to locally rotational symmetry around an impurity atom., as well as to the valley-dependent barrierlike or traplike impurity potential.

The matrix-form Dirac equation in Eq. (C7) can be solved analytically [31], yielding the solutions for $\xi \leqslant 1$,

$$
\begin{bmatrix}
\mathcal{R}_{1,\ell}^\tau(\xi) \\
\mathcal{R}_{2,\ell}^\tau(\xi) \\
\mathcal{R}_{3,\ell}^\tau(\xi)
\end{bmatrix}
=
\begin{bmatrix}
\cos\phi\, J_{\ell-\tau}(\xi\eta_0^\tau) \\
iS_0^\tau\, J_\ell(\xi\eta_0^\tau) \\
-\sin\phi\, J_{\ell+\tau}(\xi\eta_0^\tau)
\end{bmatrix},
\quad \text{(C9)}
$$

where $\eta_0^\tau(k_\parallel) = |E_0(k_\parallel) - \tau V_0|r_0/\hbar v_F$, and $S_0^\tau = \mathrm{sgn}[E_0(k_\parallel) - \tau V_0]$ with $(S_0^\tau)^2 = 1$.

Now we turn to the calculation of $\bar{\tau}_\phi(k_F, \tau)$. From Eq. (C2) we get

$$
\mathcal{W}_{\mathrm{in}}^{\tau,\phi}(k_\parallel) = \frac{n_i}{2\pi\hbar^2 v_F} k_\parallel f_{k_\parallel} \sum_\pm \int_{-\pi}^\pi d\beta_s\, |\cos\theta| \left| \frac{U_0^\tau(2k_\parallel|\cos\theta|)}{\epsilon_\phi(2k_\parallel|\cos\theta|)} \right|^2 |\mathcal{F}_{\tau,\phi}(k_\parallel,\beta_s)|^2,
\quad \text{(C10)}
$$

where $|\cos\theta| = |\sin(|\beta_s|/2)|$, $n_i = N_i/\mathcal{S}$ is the areal density of ionized impurities, and the summation $\sum_\pm$ corresponds to conditions $\varepsilon_{\mathbf{k}_\parallel} = \varepsilon_{\mathbf{k}_\parallel\pm\mathbf{q}_\parallel}$ for two delta functions in Eq. (C2). Additionally, from Eq. (C5) we find for $s = +1$ that

$$
\mathcal{F}_{\tau,\phi}(k_\parallel,\beta_s) = \frac{1}{2} \sum_\ell \left\{ (-i)^{-\tau}\tau\cos\phi\,\chi_{1,\ell}^\tau(k_\parallel) + \chi_{2,\ell}^\tau(k_\parallel) + (-i)^\tau\tau\sin\phi\,\chi_{3,\ell}^\tau(k_\parallel) \right\}
$$

$$
\times \left\{ (-i)^\tau\tau\cos\phi\,\chi_{1,\ell}^\tau(k_\parallel)\, e^{i\tau\beta^s_{\mathbf{k}_\parallel,\mathbf{q}_\parallel}} - \chi_{2,\ell}^\tau(k_\parallel) + (-i)^{-\tau}\tau\sin\phi\,\chi_{3,\ell}^\tau(k_\parallel)\, e^{-i\tau\beta^s_{\mathbf{k}_\parallel,\mathbf{q}_\parallel}} \right\}
$$

$$
\equiv \kappa_0(k_\parallel,\phi,\tau) + \kappa_1(k_\parallel,\phi,\tau)\, e^{i\tau\beta_s} + \kappa_2(k_\parallel,\phi,\tau)\, e^{-i\tau\beta_s} + \kappa_3(k_\parallel,\phi,\tau)(1 + e^{i\tau\beta_s})
$$

$$
+ \kappa_4(k_\parallel,\phi,\tau)(1 + e^{-i\tau\beta_s}) + \kappa_5(k_\parallel,\phi,\tau)\cos(\tau\beta_s),
\quad \text{(C11)}
$$

where

$$
\begin{Bmatrix}
\chi_{1,\ell}^\tau(k_\parallel) \\
\chi_{2,\ell}^\tau(k_\parallel) \\
\chi_{3,\ell}^\tau(k_\parallel)
\end{Bmatrix}
= \sqrt{2\pi} \left\{ \int_0^1 d\xi\, \xi \left[\cos^2\phi J_{\ell-\tau}^2(\xi\eta_0^\tau) + J_\ell^2(\xi\eta_0^\tau) + \sin^2\phi J_{\ell+\tau}^2(\xi\eta_0^\tau) \right] \right\}^{-1/2}
$$

$$
\times
\begin{Bmatrix}
\cos\phi \\
iS_0^\tau \\
-\sin\phi
\end{Bmatrix}
\int_0^1 d\xi\, \xi
\begin{Bmatrix}
J_{\ell-\tau}(k_\parallel r_0\xi)J_{\ell-\tau}(\xi\eta_0^\tau) \\
J_\ell(k_\parallel r_0\xi)J_\ell(\xi\eta_0^\tau) \\
J_{\ell+\tau}(k_\parallel r_0\xi)J_{\ell+\tau}(\xi\eta_0^\tau)
\end{Bmatrix},
\quad \text{(C12)}
$$

and six real coefficients κ_i for $i = 0, 1, \ldots, 5$ are given by

$$\kappa_0(k_\parallel, \phi, \tau) = \frac{1}{2} \sum_{\ell=-\infty}^{\infty} |\chi_{2,\ell}^\tau(k_\parallel)|^2, \quad \kappa_1(k_\parallel, \phi, \tau) = \frac{1}{2} \cos^2\phi \sum_{\ell=-\infty}^{\infty} [\chi_{1,\ell}^\tau(k_\parallel)]^2,$$

$$\kappa_2(k_\parallel, \phi, \tau) = \frac{1}{2} \sin^2\phi \sum_{\ell=-\infty}^{\infty} [\chi_{3,\ell}^\tau(k_\parallel)]^2, \quad \kappa_3(k_\parallel, \phi, \tau) = -\frac{i}{2} \cos\phi \sum_{\ell=-\infty}^{\infty} \chi_{1,\ell}^\tau(k_\parallel) \chi_{2,\ell}^\tau(k_\parallel),$$

$$\kappa_4(k_\parallel, \phi, \tau) = +\frac{i}{2} \sin\phi \sum_{\ell=-\infty}^{\infty} \chi_{2,\ell}^\tau(k_\parallel) \chi_{3,\ell}^\tau(k_\parallel), \quad \kappa_5(k_\parallel, \phi, \tau) = -\frac{1}{2} \sin 2\phi \sum_{\ell=-\infty}^{\infty} \chi_{1,\ell}^\tau(k_\parallel) \chi_{3,\ell}^\tau(k_\parallel). \tag{C13}$$

Then, at low T, from the detailed-balance condition and Eq. (C10) we finally arrive at

$$\frac{1}{\bar{\tau}_\phi(k_F, \tau)} = \frac{4}{\rho_0 \mathcal{S}} \sum_{\mathbf{k}_\parallel} \frac{f_T^{(0)}[\varepsilon(k_\parallel)]}{\tau_\phi(\mathbf{k}_\parallel, \tau)} = \frac{4}{\rho_0 \mathcal{S}} \sum_{\mathbf{k}_\parallel} \mathcal{W}_{\text{in}}^{\tau,\phi}(k_\parallel) \, \Theta(k_F - k_\parallel)$$

$$= \frac{4n_i}{\pi^2 \hbar^2 v_F \rho_0} \int_{-\pi}^{\pi} d\beta_s \, |\cos\theta| \int_0^{k_F} dk_\parallel \, k_\parallel^2 \left| \frac{U_0^\tau(2k_\parallel |\cos\theta|)}{\epsilon_\phi(2k_\parallel |\cos\theta|)} \right|^2 |\mathcal{F}_{\tau,\phi}(k_\parallel, \beta_s)|^2. \tag{C14}$$

APPENDIX D: INVERSE MOMENTUM-RELAXATION-TIME TENSOR

The inverse momentum-relaxation-time tensor $\overset{\leftrightarrow}{\mathcal{T}}_p^{-1}(\tau, \phi)$ introduced in Eq. (9) comes from the statistically averaged resistive forces $\boldsymbol{f}_i(\tau, \phi)$ due to scattering of electrons by ionized impurities (i) at low temperatures [37,38].

For electrons moving with a center-of-mass momentum $\hbar \boldsymbol{K}_0^{\tau,\phi}$, the resistive force $\boldsymbol{f}_i(\tau, \phi)$ from impurity scattering is calculated as [41]

$$\boldsymbol{f}_i(\tau, \phi) = -N_i \left(\frac{2\pi}{\hbar} \right) \frac{v_F}{k_F} \sum_{\mathbf{k}_\parallel, \mathbf{q}_\parallel} \hbar \boldsymbol{q}_\parallel (\hbar \boldsymbol{q}_\parallel \cdot \boldsymbol{K}_0^{\tau,\phi}) \left| U_{\text{im}}^{\tau,\phi}(\boldsymbol{q}_\parallel, \boldsymbol{k}_\parallel) \right|^2 \left(-\frac{\partial f_{\mathbf{k}_\parallel}}{\partial \varepsilon_{\mathbf{k}_\parallel}} \right) \delta(\varepsilon_{\mathbf{k}_\parallel + \mathbf{q}_\parallel} - \varepsilon_{\mathbf{k}_\parallel}), \tag{D1}$$

and we have $\overset{\leftrightarrow}{\mathcal{T}}_i^{-1}(\tau, \phi) \cdot \boldsymbol{K}_0^{\tau,\phi} = -\boldsymbol{f}_i(\tau, \phi)/N_0\hbar$ by definition. This leads to

$$\overset{\leftrightarrow}{\mathcal{T}}_i^{-1}(\tau, \phi) = \frac{2\pi N_i v_F}{N_0 k_F} \sum_{\mathbf{k}_\parallel, \mathbf{q}_\parallel} \left| U_{\text{im}}^{\tau,\phi}(\boldsymbol{q}_\parallel, \boldsymbol{k}_\parallel) \right|^2 \left(-\frac{\partial f_{\mathbf{k}_\parallel}}{\partial \varepsilon_{\mathbf{k}_\parallel}} \right) \delta(\varepsilon_{\mathbf{k}_\parallel + \mathbf{q}_\parallel} - \varepsilon_{\mathbf{k}_\parallel}) [\boldsymbol{q}_\parallel \otimes \boldsymbol{q}_\parallel^T], \tag{D2}$$

where $[\boldsymbol{q}_\parallel \otimes \boldsymbol{q}_\parallel^T] \equiv \begin{bmatrix} q_x^2 & q_x q_y \\ q_y q_x & q_y^2 \end{bmatrix}$. Finally, the inverse momentum-relaxation-time tensor is simply given by $\overset{\leftrightarrow}{\mathcal{T}}_p^{-1}(\tau, \phi) = \overset{\leftrightarrow}{\mathcal{T}}_i^{-1}(\tau, \phi)$ after neglecting phonon scattering at low T.

Furthermore, at low T, from Eqs. (D1) and (D2) we find

$$\overset{\leftrightarrow}{\mathcal{T}}_p^{-1}(k_F, \tau, \phi) = \frac{2\pi n_i}{\rho_0} \left(\frac{v_F}{k_F} \right) \sum_{\mathbf{k}_\parallel, \mathbf{q}_\parallel} \left| U_{\text{im}}^{\tau,\phi}(\boldsymbol{q}_\parallel, \boldsymbol{k}_\parallel) \right|^2 \delta(\varepsilon_{\mathbf{k}_\parallel} - E_F) \, \delta(\varepsilon_{\mathbf{k}_\parallel + \mathbf{q}_\parallel} - \varepsilon_{\mathbf{k}_\parallel}) \left[\boldsymbol{q}_\parallel \otimes \boldsymbol{q}_\parallel^T \right]$$

$$= \frac{4n_i k_F^3}{\pi^2 \hbar^2 v_F \rho_0} \int_{-\pi}^{\pi} d\beta_s \, |\cos\theta| \cos^2\theta \left| \frac{U_0^\tau(2k_F |\cos\theta|)}{\epsilon_\phi^2(2k_F |\cos\theta|)} \right|^2 |\mathcal{F}_{\tau,\phi}(k_F, \beta_s)|^2 \begin{bmatrix} \cos^2\theta & \cos\theta \sin\theta \\ \sin\theta \cos\theta & \sin^2\theta \end{bmatrix}, \tag{D3}$$

where $\epsilon_\phi(q_\parallel)$ is the static dielectric function, $|\mathcal{F}_{\tau,\phi}(k_F, \beta_s)|^2$ is given by Eq. (C11), $\cos\theta = -\sin(|\beta_s|/2)$, $\sin\theta = \text{sgn}(\beta_s) \cos(|\beta_s|/2)$ for $-\pi \leqslant \beta_s \leqslant \pi$, and $\text{sgn}(x)$ is a sign function.

APPENDIX E: MOBILITY TENSOR

From the force-balance equation in Eq. (9), we get the following set of linear equations [38] for center-of-mass wave vector $\boldsymbol{K}_0^{\tau,\phi} = \{K_x^{\tau,\phi}, K_y^{\tau,\phi}\}$, i.e.,

$$b_{xx}(\tau, \phi)K_x^{\tau,\phi} + \left[b_{xy}(\tau, \phi) - \frac{q_0 v_F B_z}{\hbar k_F} \right] K_y^{\tau,\phi} = \frac{q_0}{\hbar} E_x, \tag{E1}$$

$$\left[b_{yx}(\tau, \phi) + \frac{q_0 v_F B_z}{\hbar k_F} \right] K_x^{\tau,\phi} + b_{yy}(\tau, \phi)K_y^{\tau,\phi} = \frac{q_0}{\hbar} E_y, \tag{E2}$$

where we have used the notations $\boldsymbol{B}_\perp = \{0, 0, B_z\}$, $\boldsymbol{E}_\parallel = \{E_x, E_y, 0\}$, $q_0 = -e$, and have written the matrix $\overleftrightarrow{\mathcal{T}}_p^{-1}(\tau, \phi) \equiv \{b_{ij}(\tau, \phi)\}$ for $i, j = x, y$. By defining the determinant of the coefficient matrix in Eqs. (E1) and (E2) as $\mathrm{Det}\{\overleftrightarrow{\mathcal{C}}_{\tau,\phi}\}$, i.e.,

$$\mathrm{Det}\{\overleftrightarrow{\mathcal{C}}_{\tau,\phi}\} = b_{xx}(\tau, \phi)\, b_{yy}(\tau, \phi) - \left[b_{xy}(\tau, \phi) - \frac{q_0 v_F B_z}{\hbar k_F}\right]\left[b_{yx}(\tau, \phi) + \frac{q_0 v_F B_z}{\hbar k_F}\right], \tag{E3}$$

as well as the source vector $\boldsymbol{s}$, given by

$$\boldsymbol{s} = \begin{bmatrix} \dfrac{q_0}{\hbar}\, E_x \\[2mm] \dfrac{q_0}{\hbar}\, E_y \end{bmatrix}, \tag{E4}$$

we can reduce this linear equations to a matrix form $\overleftrightarrow{\mathcal{C}}_{\tau,\phi} \cdot \boldsymbol{K}_0^{\tau,\phi} = \boldsymbol{s}$ with the formal solution $\boldsymbol{K}_0^{\tau,\phi} = \overleftrightarrow{\mathcal{C}}_{\tau,\phi}^{-1} \cdot \boldsymbol{s}$. Explicitly, we find the solution $\boldsymbol{K}_0^{\tau,\phi} = \{K_x^{\tau,\phi}, K_y^{\tau,\phi}\}$ for $j = x, y$ from

$$K_j^{\tau,\phi} = \frac{\mathrm{Det}\{\overleftrightarrow{\Delta}_j^{\tau,\phi}\}}{\mathrm{Det}\{\overleftrightarrow{\mathcal{C}}_{\tau,\phi}\}}, \tag{E5}$$

where

$$\mathrm{Det}\{\overleftrightarrow{\Delta}_1^{\tau,\phi}\} = \frac{q_0}{\hbar}\, E_x\, b_{yy}(\tau, \phi) - \frac{q_0}{\hbar}\, E_y\left[b_{xy}(\tau, \phi) - \frac{q_0 v_F B_z}{\hbar k_F}\right], \tag{E6}$$

$$\mathrm{Det}\{\overleftrightarrow{\Delta}_2^{\tau,\phi}\} = \frac{q_0}{\hbar}\, E_y\, b_{xx}(\tau, \phi) - \frac{q_0}{\hbar}\, E_x\left[b_{yx}(\tau, \phi) + \frac{q_0 v_F B_z}{\hbar k_F}\right]. \tag{E7}$$

Even in the case of $E_y = 0$, the transverse center-of-mass wave number $K_y^{\tau,\phi}$ can still be nonzero due to an external magnetic field B_z or by nonzero off-diagonal element b_{yx} of the inverse momentum-relaxation-time tensor. The mobility tensor $\overleftrightarrow{\mu}_{\tau,\phi} = \{\mu_{ij}^{\tau,\phi}\}$ can be simply obtained from $\mu_{ij}^{\tau,\phi} = (v_F/k_F)\,(\partial K_i^{\tau,\phi}/\partial E_j)$.

---

[1] S. D. Bader and S. S. P. Parkin, Ann. Rev. Condens. Matter. Phys. **1**, 71 (2010).

[2] A. Rycerz, J. Tworzydlo, and C. W. J. Beenakker, Nat. Phys. **3**, 172 (2007).

[3] D. Xiao, W. Yao, and Q. Niu, Phys. Rev. Lett. **99**, 236809 (2007).

[4] K. Behnia, Nat. Nanotech. **7**, 488 (2012).

[5] C. E. Nebel, Nat. Mater. **12**, 690 (2013).

[6] R. V. Gorbachev, J. C. W. Song, G. L. Yu, A. V. Kretinin, F. Withers, Y. Cao, A. Mishchenko, I. V. Grigorieva, K. S. Novoselov, L. S. Levitov, and A. K. Geim, Science **346**, 448 (2014).

[7] X. Xu, W. Yao, D. Xiao, and T. F. Heinz, Nat. Phys. **10**, 343 (2014), review.

[8] A. Kundu, H. A. Fertig, and B. Seradjeh, Phys. Rev. Lett. **116**, 016802 (2016).

[9] Y. Ye, J. Xiao, H.-L. Wang, Z.-L. Ye, H.-Y. Zhu, M. Zhao, Y. Wang, J.-H. Zhao, X.-B. Yin, and X. Zhang, Nat. Nanotech. **11**, 598 (2016).

[10] J. Lu, C. Qiu, M. Ke, and Z. Liu, Phys. Rev. Lett. **116**, 093901 (2016).

[11] F. Delgado and J. Fernández-Rossier, Phys. Rev. Lett. **108**, 196602 (2012).

[12] D. C. Tsui and G. Kaminsky, Phys. Rev. Lett. **42**, 595 (1979).

[13] K. Lai, W. Pan, D. C. Tsui, S. Lyon, M. Mühlberger, and F. Schäffler, Phys. Rev. Lett. **96**, 076805 (2006).

[14] Y. P. Shkolnikov, E. P. De Poortere, E. Tutuc, and M. Shayegan, Phys. Rev. Lett. **89**, 226805 (2002).

[15] K. S. Novoselov, A. K. Geim *et al.*, Sci. **306**, 666 (2004).

[16] K. F. Mak, K. L. McGill, J. Park, and P. L. McEuen, Science **344**, 1489 (2014).

[17] N. Nagaosa, J. Sinova, S. Onoda, A. H. MacDonald, and N. P. Ong, Rev. Mod. Phys. **82**, 1539 (2010).

[18] J. Sinova, S. O. Valenzuela, J. Wunderlich, C. H. Back, and T. Jungwirth, Rev. Mod. Phys. **87**, 1213 (2015).

[19] A. Raoux, M. Morigi, J.-N. Fuchs, F. Piéchon, and G. Montambaux, Phys. Rev. Lett. **112**, 026402 (2014).

[20] J. D. Malcolm and E. J. Nicol, Phys. Rev. B **93**, 165433 (2016).

[21] B. Dey and T. K. Ghosh, Phys. Rev. B **98**, 075422 (2018).

[22] K. Novoselov, A. K. Geim, S. Morozov, D. Jiang, M. Katsnelson, I. Grigorieva, S. Dubonos, and A. Firsov, Nature (London) **438**, 197 (2005).

[23] R. R. Nair, P. Blake, A. N. Grigorenko, K. S. Novoselov, T. J. Booth, T. Stauber, N. M. Peres, and A. K. Geim, Science **320**, 1308 (2008).

[24] A. C. Ferrari, J. C. Meyer, V. Scardaci, C. Casiraghi, M. Lazzeri, F. Mauri, S. Piscanec, D. Jiang, K. S. Novoselov, S. Roth, and A. K. Geim, Phys. Rev. Lett. **97**, 187401 (2006).

[25] R. A. Vicencio, C. Cantillano, L. Morales-Inostroza, B. Real, C. Mejía-Cortés, S. Weimann, A. Szameit, and M. I. Molina, Phys. Rev. Lett. **114**, 245503 (2015).

[26] S. Mukherjee, A. Spracklen, D. Choudhury, N. Goldman, P. Ohberg, E. Andersson, and R. R. Thomson, Phys. Rev. Lett. **114**, 245504 (2015).

[27] M. J. Ablowitz and J. T. Cole, Phys. Rev. A **99**, 033821 (2019).

[28] S. Taie, H. Ozawa, T. Ichinose, T. Nishio, S. Nakajima, and Y. Takahashi, Sci. Adv. **1**, 1500854 (2015).

[29] X. Huang, Y. Lai, Z. H. Hang, H. Zheng, and C. T. Chan, Nat. Mater. **10**, 582 (2011).

[30] Y. Li, S. Kita, P. Munoz, O. Reshef, D. I. Vulis, M. Yin, M. Loncar, and E. Mazur, Nat. Photon. **9**, 738 (2015).

[31] H.-Y. Xu, L. Huang, D. H. Huang, and Y.-C. Lai, Phys. Rev. B **96**, 045412 (2017).

[32] D. Moldovan, M. Ramezani Masir, L. Covaci, and F. M. Peeters, Phys. Rev. B **86**, 115431 (2012).

[33] Q. Niu, M.-C. Chang, B. Wu, D. Xiao, and R. Cheng, *Physical Effects of Geometric Phases* (World Scientific, Singapore, 2017).

[34] J. M. Ziman, *Principles of the Theory of Solids*, 2nd ed. (Cambridge University Press, Cambridge, 1972).

[35] G. Sundaram and Q. Niu, Phys. Rev. B **59**, 14915 (1999).

[36] T. Biswas and T. K. Ghosh, J. Phys.: Condens. Matter **28**, 495302 (2016).

[37] D. H. Huang, G. Gumbs, and O. Roslyak, J. Mod. Opt. **58**, 1898 (2011).

[38] D. Backes, D. H. Huang, R. Mansell, M. Lanius, J. Kampmeier, D. Ritchie, G. Mussler, G. Gumbs, D. Grützmacher, and V. Narayan, Phys. Rev. B **96**, 125125 (2017).

[39] N. C. Miller, M. Grupen, K. Beckwith, D. Smithe, and J. D. Albrecht, J. Comput. Electr. **17**, 1658 (2018).

[40] D. Backes, D. H. Huang, R. Mansell, M. Lanius, J. Kampmeier, D. Ritchie, G. Mussler, G. Gumbs, D. Grützmacher, and V. Narayan, Phys. Rev. B **99**, 125139 (2019).

[41] D. H. Huang, P. M. Alsing, T. Apostolova, and D. A. Cardimona, Phys. Rev. B **71**, 195205 (2005).

[42] C. S. Mayberry, D. H. Huang, G. Balakrishnan, C. Kouhestani, N. Islam, S. R. J. Brueck, and A. K. Sharma, J. Appl. Phys. **118**, 134301 (2015).

[43] L. J. van der Pauw, Philips Res. Rep. **13**, 1 (1958).

[44] D. H. Huang, A. Iurov, F. Gao, G. Gumbs, and D. A. Cardimona, Phys. Rev. Appl. **9**, 024002 (2018).

[45] G. Gumbs and D. H. Huang, *Properties of Interacting Low-Dimensional Systems* (Wiley-VCH, Weinheim, 2011).